2019-04-01

Using GLUE to pull apart the provenance of atmospheric dust

Behrooz, RD

10.1016/j.aeolia.2018.12.001
Aeolian Research
Elsevier

Manuscript Details

Manuscript number	AEOLIA_2018_87_R2
Title	Using GLUE to pull apart the provenance of atmospheric dust
Article type	Full Length Article

Abstract

Identifying the sources of aeolian dust is a crucial step in mitigating the associated hazards. We apply a Generalized Likelihood Uncertainty Estimation (GLUE) model to constrain the uncertainties associated with sediment fingerprinting of atmospheric dust in the Sistan region on the Iran-Afghanistan border, one of the world's dustiest places. 57 dust samples were collected from the rooftop of the Zabol Department of Environmental Protection during a summer dusty period from June to October 2014, in addition to 31 surface soil samples collected from potential sources nearby, including cultivated land (n=8), uncultivated rangeland (n=7), and two dry lakes: Hamoun Puzak (n=10) and Hamoun Saberi (n=6). Dust and soil samples were analyzed for 24 tracers including 16 geochemical elements and 8 water-soluble ions. Five optimum composite fingerprints (Fe, Sr, Mn, Cr and Pb) were selected for discriminating sources by a two-stage statistical process involving a Kruskal-Wallis test and stepwise discriminant function analysis (DFA). Uncertainty ranges for source contributions of dust determined by the GLUE model showed that the dry lake Hamoun Puzak is the dominant source for all dust samples from Zabol and cultivated land is a secondary source. We found marked spatial variance in the importance of regional dry lake beds as dust sources, and temporal persistence in dust emissions from Hamoun Puzak, despite very large areas of adjacent lake beds drying during the study period. Aeolian sediment fingerprinting studies can benefit considerably from the constraints provided by modelling frameworks, such as GLUE, for quantifying the uncertainty in dust provenance data.

Keywords	Sediment fingerprinting; uncertainty; GLUE; atmospheric dust; Iran

Corresponding Author	Matt Telfer
Corresponding Author's Institution	Plymouth University
Order of Authors	Reza Dahmardeh behrooz, hamid gholami, Matt Telfer, John Jansen, Abolhassan Fathabadi

Suggested reviewers	Jan-Berend Stuut, Richard Brazier

Submission Files Included in this PDF

File Name [File Type]

AEOLIA_2018_87_R2_Sistan_comments_addressed.pdf [Response to Reviewers (without Author Details)]

AEOLIA_2018_87_R1_Title_Page.docx [Title Page (with Author Details)]

AEOLIA_2018_87_R2_Manuscript.docx [Manuscript (without Author Details)]

Figure_3_R1.eps [Figure]

Figure_4_R1.eps [Figure]

Figure_5_R1.eps [Figure]

Figure_8_R1.eps [Figure]

Figure_9_R1.eps [Figure]

Figs 1-2-6-7-10-11_R2.docx [Figure]

AEOLIA_2018_87_R1_CRediT Author statement.docx [Author Statement]

To view all the submission files, including those not included in the PDF, click on the manuscript title on your EVISE Homepage, then click 'Download zip file'.

Research Data Related to this Submission

Data set	https://data.mendeley.com/datasets/6672h2t3wb/draft?a=bf976f11-b4fa-4396-b6f0-61119f53049a

Data for: Using GLUE to pull apart the provenance of atmospheric dust

The full distributions of Generalized Likelihood Uncertainty Estimate (GLUE) modelling used in Behrooz et al (submitted, Aeolian Research, 2018)

Manuscript Details

Manuscript number AEOLIA_2018_87

Title Using GLUE to pull apart the provenance of atmospheric dust

Abstract

We apply a Generalized Likelihood Uncertainty Estimation (GLUE) model to constrain the uncertainties associated with sediment fingerprinting aimed at source contributions of atmospheric dust in the Sistan region on the Iran-Afghanistan border. Fifty seven dust samples were collected from the rooftop of the Zabol Department of Environmental Protection during a summer dusty period from 23 June to 4 October 2014 in addition to thirty one surface soil samples collected from potential sources nearby, including cultivated land (n=8), uncultivated range land (n=7), and two dry lakes: Hamoun Puzak (n=10) and Hamoun Saberi (n=6). Dust and soil samples were analyzed for 24 tracers including 16 geochemical elements and 8 water-soluble ions. Based on our results, five optimum composite fingerprints (Fe, Sr, Mn, Cr and Pb) were selected for discriminating sources by a two-stage statistical processes involving a Kruskal-Wallis test and stepwise discriminant function analysis (DFA). Uncertainty ranges for source contributions of dust determined from our GLUE methodology showed that the dry lake Hamoun Puzak is the dominant source for all 57 dust samples from Zabol and cultivated land is a secondary source. We found marked spatial variance in the importance of regional dry lake beds as dust sources, and equally notable temporal persistence in dust emissions from Hamoun Puzak, despite very large areas of adjacent lake beds drying and becoming exposed during the study period. Aeolian sediment fingerprinting studies can benefit considerably from the constraints provided by modelling frameworks, such as GLUE, for quantifying uncertainty in dust provenance data.

Submission Files Included in this PDF

File Name [File Type]

Using_GLUE_to_to_pull_apart_aeolian_dust_provenance.pdf [Manuscript (without Author Details)]

To view all the submission files, including those not included in the PDF, click on the manuscript title on your EVISE Homepage, then click 'Download zip file'.

Research Data Related to this Submission

Data set https://data.mendeley.com/datasets/6672h2t3wb/draft/b?a=YmY5NzZmMTEtYjRmYS00Mzk2LWI2ZjAtNjExMTlmNTMwNDlh

Data for: Using GLUE to pull apart the provenance of atmospheric dust

The full distributions of Generalized Likelihood Uncertainty Estimate (GLUE) modelling used in Behrooz et al (submitted, Aeolian Research, 2018)

Using GLUE to pull apart the provenance of atmospheric dust

HIGHLIGHTS

- The GLUE model is applied to reveal the provenance of aeolian dust in Zabol, Iran.
- Quantitative estimates and uncertainties of four different dust sources are distinguished.
- One dry lake, Hamoun Puzak, is by far the dominant dust source, despite others nearby.
- The major dust source is insensitive to large changes in exposed local dry lake beds.
- Cultivated land is the second most important dust source, ahead of some playas.

Abstract

We apply a Generalized Likelihood Uncertainty Estimation (GLUE) model to constrain the uncertainties associated with sediment fingerprinting aimed at source contributions of atmospheric dust in the Sistan region on the Iran-Afghanistan border. Fifty seven dust samples were collected from the rooftop of the Zabol Department of Environmental Protection during a summer dusty period from 23 June to 4 October 2014 in addition to thirty one surface soil samples collected from potential sources nearby, including cultivated land (n=8), uncultivated range land (n=7), and two dry lakes: Hamoun Puzak (n=10) and Hamoun Saberi (n=6). Dust and soil samples were analyzed for 24 tracers including 16 geochemical elements and 8 water-soluble ions. Based on our results, five optimum composite fingerprints (Fe, Sr, Mn, Cr and Pb) were selected for discriminating sources by a two-stage statistical processes involving a Kruskal-Wallis test and stepwise discriminant function analysis (DFA). Uncertainty ranges for source contributions of dust determined from our GLUE methodology showed that the dry lake Hamoun Puzak is the dominant source for all dust samples from Zabol and cultivated land is a secondary source. We found marked spatial variance in the importance of regional dry lake beds as dust sources, and equally notable temporal persistence in dust emissions from Hamoun Puzak, despite very large areas of adjacent lake beds drying and becoming exposed during the study period. Aeolian sediment fingerprinting studies can benefit considerably from the constraints provided by modelling frameworks, such as GLUE, for quantifying uncertainty in dust provenance data.

KEY WORDS: sediment fingerprinting, uncertainty, GLUE, atmospheric dust, Iran

1. Introduction

Constraining the source of atmospheric dust particles circulating in the ancient past as well as the present-day is central to understanding the manifold implications of dust in the Earth system (Ridgwell, 2002; Goudie and Middleton, 2006; Shao et al., 2011). Ancient dust deposits are archives of long-term environmental change (Dietze et al., 2016); the best-known and longest being the >8 Myr loess record in China (Sun & Zhu 2010). Present-day dust storms trigger a series of negative off-site and on-site repercussions (Goossens, 2003). Off-site effects include respiratory disease in humans and non-humans, contamination of food and water supplies, and interference with traffic safety, machinery, and electronics. On-site effects include the loss of soil organic matter, nutrients, and overall agricultural productivity (Goudie and Middleton, 2006). From this perspective, identifying sources of dust and quantifying multi-source contributions and their uncertainties is a key step towards hazard mitigation, especially in drylands.

A diverse range of techniques have been employed for tracing sources of atmospheric dust, including isotopic ratios (e.g., Krom et al., 1999; Nakano et al., 2004; Grousset and Biscaye, 2005; Chen et al., 2007; Cao et al., 2008; Wang et al., 2005; Rio-Salas et al., 2012; Yang et al., 2009); mineralogical and chemical characteristics (Shen et al., 2009); meteorological data (Rezazadeh et al., 2013; Nabavi et al., 2016; Ge et al., 2016; Rashki et al., 2017); synthesis of isotopic and geochemical data (e.g., Aarons et al., 2017; Wei et al., 2017; Chavagnac et al., 2008); synthesis of trace element and water-soluble ion analyses (Dahmardeh Behrooz et al., 2017a,b); numerical simulation (Hamidi et al., 2014; Nabavi et al., 2017); satellite data (Long et al., 2016; Cherboudj et al., 2016; Schepanski et al., 2012); and multidisciplinary approaches (Yan et al., 2015; Cao et al., 2015). While most of the studies listed above are highly successful at inferring dust sources, we note that in many cases the uncertainties associated with ascribing provenance are not considered formally. We see this an important omission for two reasons: 1) airborne dust is commonly generated simultaneously from multiple populations and areas of fine-grained particles; and 2) these multiple populations are, in turn, typically an amalgam generated from different sources and mixed to differing degrees over timescales ranging from geological to individual storm events. In other words, dust provenance presents a diabolical mixing-problem and hence uncertainty is fundamental. These two points ultimately stem from geomorphic processes of fine-particle production, transport, deposition, and reworking.

Sediment fingerprinting is widely used to quantify source contributions of fluvial sediments (e.g., Collins et al., 1997; Walling, 2005; Stone et al., 2014; Zhou et al., 2016a; and Manjoro et al., 2017) and its application to aeolian problems is growing (e.g., Liu et al., 2016; and Gholami et al., 2017a,b). Moreover, the uncertainties involved with this method are gaining increased attention (Walling, 2013). In order to manage and quantify the uncertainty in fluvial sediment fingerprinting, some studies have applied a Monte Carlo simulation framework (e.g., Motha et al., 2003; Collins et al., 2012; Voli et al., 2013; Smith and Blake, 2014; Stone et al., 2014; Sherriff et al., 2015; and Vale et al., 2016). Similarly, Bayesian approaches are also applied to fingerprinting aeolian sands (Gholami et al., 2017b) and fluvial sediments (e.g., Massoudieh et al., 2013; Cooper et al., 2014; Cooper et al., 2015; Stewart et al., 2015; and Abban et al., 2016). Yet, several challenges remain in adequately capturing the uncertainty associated with diverse aeolian dust sources and pathways (Walling, 2013) and we suggest that techniques developed in other disciplines may offer a way forward (Gholami et al., 2017b).

First proposed for hydrological modelling by Beven and Binley (1992), GLUE (Generalised Likelihood Uncertainty Estimation) has gained much favour as a tool for evaluating uncertainty estimates (e.g., Hassan et al., 2008; Zhou et al., 2016b; Viola et al., 2009; Mantovan and Todini, 2006; and Gong et al., 2011). Here, we apply GLUE to the problem of dust provenance in the Sistan Hamoun region on the Iran-Afghanistan border. Since it constitutes a major dust source for south-west Asia, Sistan has been the focus of numerous previous investigations, (e.g., Goudie and Middleton, 2006; Rashki et al., 2012, 2013 a,b, 2015; Alizadeh Choobari et al., 2014). Recent work has generated an important geochemical dataset of dust samples from a meteorological station at Zabol which has been analyzed geochemically to provide qualitative estimates of source (Dahmardeh Behrooz et al., 2017a) and the temporal variability of dust emissions (Dahmardeh Behrooz et al., 2017b). Here we provide the first attempt to formally quantify aeolian dust provenance and associated uncertainties with this dataset using GLUE (Dahmardeh Behrooz et al., 2017a; 2017b).

2. Study area

The Sistan-Hamoun study area (Fig. 1) straddles the border between Afghanistan and the Sistan and Baluchestan province of south-eastern Iran (30˚5′ to 31˚28′ N and 61˚15′ to 61˚50′ E) (Rashki et al., 2012, 2013a). The Hamoun lakes complex comprises three main lakes: Hamoun Hirmand, Hamoun Saberi, and Hamoun Puzak, which are recharged primarily from Afghanistan by the Hirmand (Helmand) River with smaller contributions from streams to the north and west (Esmaeili and Omrani, 2007). Following exceptionally high runoff, the lakes form a single body of water ~5700 km^2 in area

and ~13 Mm^3 in volume (Sharifikia, 2013), though such events have become rare in recent decades while dust emissions have grown correspondingly in magnitude (Goudie and Middleton, 2006; Rashki et al., 2012).

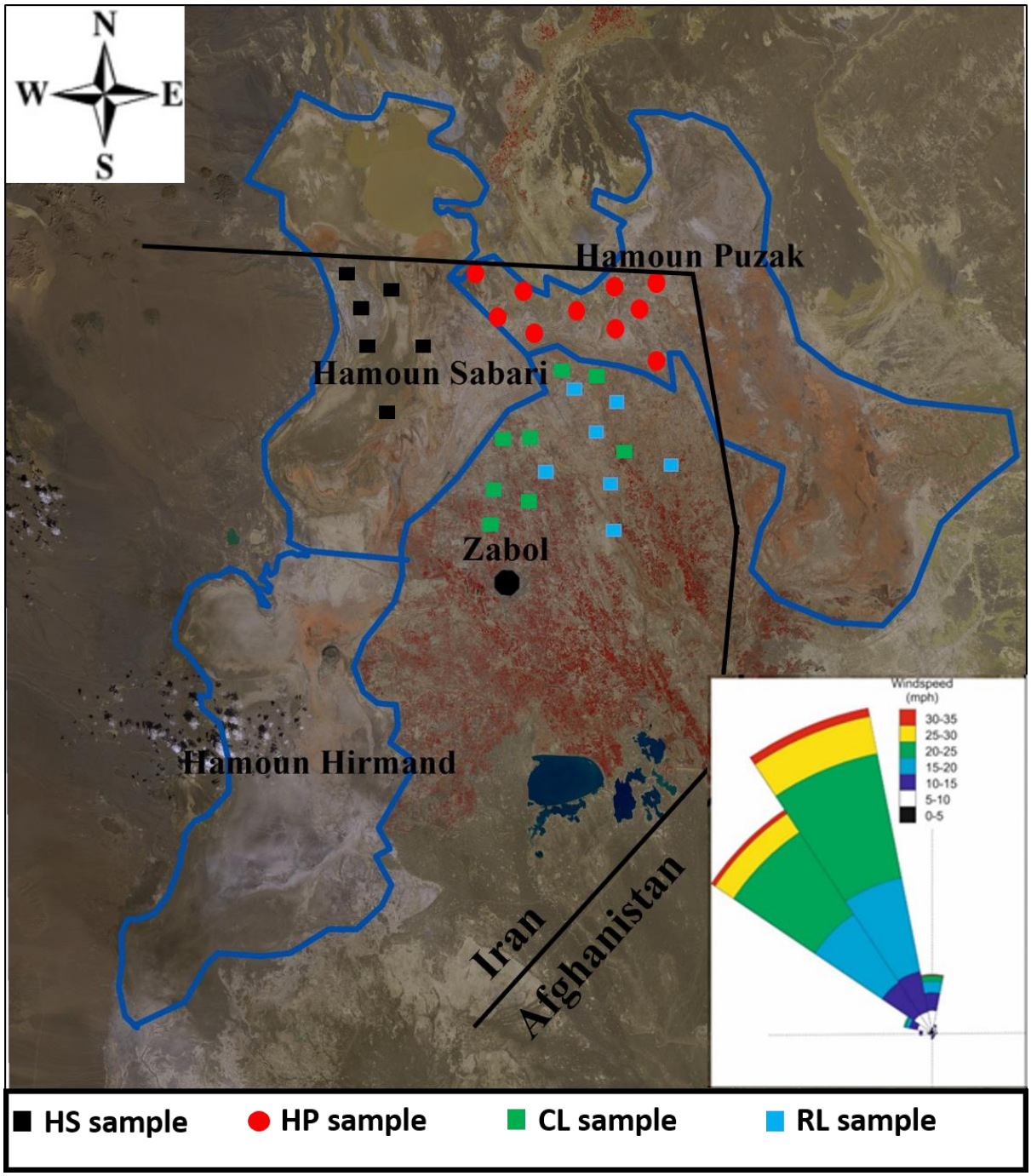

Figure 1: Sampling sites in the Sistan region: the dry-bed of Hamoun Puzak (HP); the dry-bed of Hamoun Saberi (HS); uncultivated range land (RL); and cultivated land (CL). Inset shows the hourly averaged wind regime for the period June-October 2014 (data source: National Climatic Data Centre, Climate Data Online).

The climate of the Sistan region is arid to hyper-arid, and land-use is chiefly linked to agriculture and fishing. At Zabol meteorological station (Fig. 1), mean rainfall is 55 mm/y and mean evaporation is

>4000 mm/y (Moghaddamnia et al., 2009). The prevailing wind is the notorious "Wind of 120 Days" from the north, which in the summer is accelerated into a Low-Level Jet (LLJ) by a persistent high-pressure system over the Hindu Kush and the channeling effect of the surrounding topography (Alizadeh-Choobari et al., 2014). As a result, the city of Zabol and its ~135,000 inhabitants experience dust storms of catastrophic proportions, resulting in Zabol ranking as the world's most polluted city for particulate matter less than 2.5 µm (PM2.5) in size (World Health Organisation, 2016).

3. Methods

3.1 Field sampling

We set out to characterise the soil materials for four different potential sources of atmospheric dust emissions to the north of Zabol city (Fig. 1): 1) the dry lake-bed of Hamoun Puzak (Fig. 2a); 2) the dry lake-bed of Hamoun Saberi (Fig. 2b); 3) cultivated arable farmland generally without crop-cover in summer (Fig. 2c); and 4) bare land surfaces with sparse to negligible natural vegetation cover (Fig. 2d). A total of 31 surficial soil samples (<5 cm depth in a 30 cm^2 area) were collected from the four potential sources (Table 1). We sieved the soil samples with a 400-mesh sieve, retaining particles with a nominal geometric diameter of < 38.5 µm, which is equivalent to the aerodynamic diameter of dust (Cao et al., 2008). After sieving we retained about 5 g of dust-sized material from each sample.

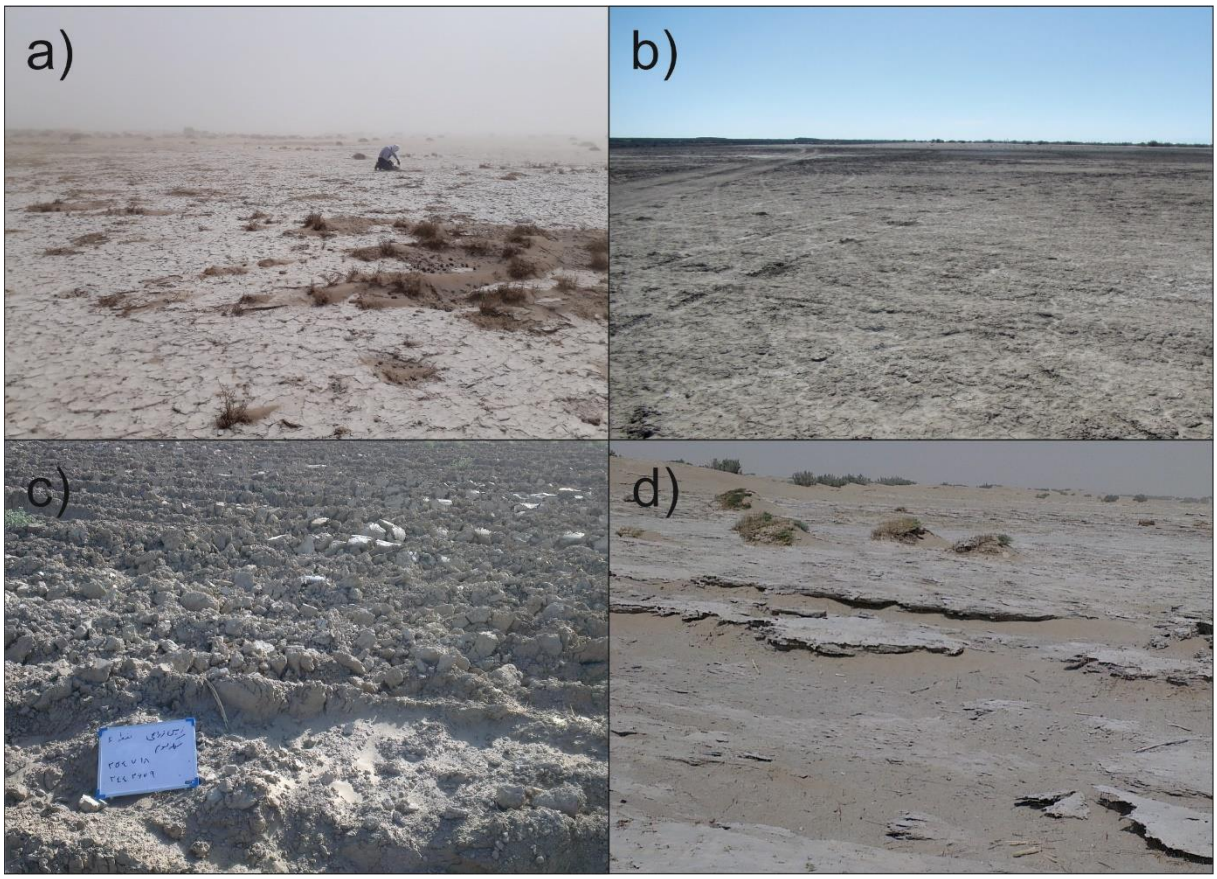

Figure 2. Typical examples of the land surfaces we sampled. a) Hamoun Puzak dry lake-bed, b) Hamoun Saberi dry lake-bed, c) close-up view of cultivated agricultural land surface during the summer months, and d) sparsely vegetated, uncultivated rangeland.

During an exceptionally dusty summer period in Zabol (23 June to 4 October 2014), 57 atmospheric dust samples were collected at one- to four day intervals (Table 1) with sampling apparatus fitted to the rooftop of the Department of Environmental Protection (5 m above ground level, 31˚N, 61.3˚E) in an outer suburban area with no major industrial activities nor local fugitive dust sources. Our two dust samplers (Model Chrono, Zambelli, Milan) were equipped with cyclones operating at a flow rate of 16.7 L/min as per the EU norms (Dahmardeh Behrooz et al, 2017a; 2017b). Total suspended-particle (TSP) samples were collected in Teflon filters (0.45 µm pore size and 47 mm diameter) and then desiccated for 24-hours at 25 °C. Dust mass concentrations were measured gravimetrically by weighing the Teflon filters before and after sampling using an analytical balance (Adam model) with ±0.1 mg precision. We refrigerated all dust samples at 4˚C until chemical analysis (Dahmardeh Behrooz et al., 2017 a).

3.2 Laboratory analysis of water-soluble ions and trace elements

We measured the concentrations of 8 water-soluble ions in our samples (viz., Na^+, NH^+_4, K^+, Ca^{2+}, Mg^{2+}, Cl^-, NO^-_3, NO^-_2). Three cations (Na^+, NH^+_4 and K^+) were measured with a Shim-pack IC-C1 (Shimadzu DGU-12A) using 5-mM HNO_3 solution as eluent. Three anions (Cl^-, NO^-_3 and NO^-_2) were measured with a Shim-pack ICA1 (Shimadzu DGU-12A), using 2.5–mM phthalic acid combined with 2.4-mM tris-(hydroxymethyl) aminomethane as eluent (Lin, 2002). Two cations (Ca^{2+} and Mg^{2+}) were measured via flame atomic absorption spectrometry (Philips, PU9400X, England).

After acid digestion, all samples were analyzed to determine the concentrations of 16 trace elements (viz., Al, As, Au, Co, Cr, Cu, Fe, Li, Mg, Mn, Ni, Pb, Pt, Sn, Sr, and Zn) via Inductively Coupled Plasma Atomic Emission Spectroscopy (ICP-OES, Perkine Elmer, Optima 2000, USA). Further details of sampling and laboratory procedures are given in Dahmardeh Behrooz et al. (2017a,b).

3.3 Two-stage method: Kruskal-Wallis test and discriminant function analysis

Our measurements of 8 water-soluble ions and 16 trace elements form the basis of the sediment fingerprinting method aimed at identifying the source contribution of the Zabol dust samples. We adopt a two-stage statistical procedure following the approach of Collins et al. (1997). In stage one we tested the primary ability of tracers to discriminate dust sources using the Kruskal-Wallis H test.

Tracers with critical values at the 95 % confidence levels or better were taken to the second stage in which we identified optimum composite fingerprints using a stepwise discriminant function analysis based on minimization of Wilk's lambda.

3.4 Generalised Likelihood Uncertainty Estimation (GLUE)

GLUE was first devised by Beven and Binley (1992) as a means of sensitivity analysis and uncertainty estimation in environmental model outputs. We use GLUE to quantify the uncertainty in the sediment fingerprinting results via the following five steps:

1) Random sampling of parameter sets (300,000 iterations) are conducted using the Latin Hypercube Sampling (LHS) method (Zhou et al, 2016b) and assuming source contributions from each source are non-negative and total contributions sum to unity. Due to the lack of prior information, we used a uniform distribution as the prior distribution for all parameters.

2) Selection of a likelihood function and behavioral parameter thresholds. Here, we adopt the Nash–Sutcliffe coefficient (ENS) as the likelihood function (Jin et al, 2010):

$$ME = 1 - \frac{\sum(O_{obs} - O_{sim})}{\sum(O_{obs} - \hat{Q}_{obs})} = 1 - \frac{\sigma_i^2}{\sigma_{obs}^2} \quad \text{(eq.1)},$$

where $\hat{Q}_{obs}$ is the mean value of the observed tracer concentration; O_{sim} is the simulated tracer concentration; O_{obs} is the observed tracer concentration; σ^2_i is the error variance for the *i*th model (i.e., the combination of the model and the *i*th parameter set) and σ^2_{obs} is the variance of the observations.

3) Sampled parameter sets from step 1 are input to the mixing model (equation 2) and the likelihood function is calculated for each parameter set as:

$$C_{dust} = C_{Sources} \times P \quad \text{(eq. 2)}$$

where P is an m dimensional column vector of sources contribution (sampled parameter sets), C_{dust} is an n-dimensional column vector of element concentration in sediment sample, $C_{Sources}$ is an n×m-dimensional matrix representing mean tracer concentration in sources (each row represents mean tracer concentration in each source), where n is the number of optimum composite fingerprints (n=5) and m is the number of dust sources (m=4).

4) Parameter sets are divided into behavioural and nonbehavioural types with respect to a threshold value (Zhou et al, 2016). In this step, those parameter sets that have likelihood functions greater than a threshold value were classified as behavioural parameter sets. For the next step, nonbehavioural parameter sets were discarded.

5) For behavioural parameter sets, likelihood weights are rescaled such that they sum to one, then each parameter is sorted and we calculate cumulative distributions for each parameter. Quintiles and uncertainty intervals are calculated via the cumulative distributions.

3.5 Geospatial analysis and climate data

Landsat data were downloaded from the United States Geological Survey's Earth Explorer, and all analysis was conducted within ArcGIS 10.3. Quantitative analysis of water extent was conducted using a modified Normalized Difference Water Index (NDWI), based on the green (Band 3) and short-wave infrared (Band 6) bands of Landsat 8 data (Xu, 2006). Climate data are taken from the Hourly Global Surface Data (DS3505) dataset for the Zabol station (World Meteorological Organization ID: 40829), accessed via the legacy Climate Data Online (CDO) portal of the National Oceanic and Atmospheric Administration's (NOAA) National Climatic Data Centre (NCDC) online (available at https://www7.ncdc.noaa.gov/CDO/dataproduct).

4. Results

4.1 Kruskal-Wallis test and discriminant function analysis

The results of the Kruskal-Wallis tests (Table 2) indicate that among the twenty-four measured properties (8 water-soluble ions and 16 element concentrations), thirteen trace elements (Mg, Sr, Li, Fe, Cr, Cu, As, Ni, Pb, Mn, and Sn) and one ion (Ca^{2+}) show statistically significant differences at the 95 %-level between our four potential dust sources (the two dry lake beds, cultivated farmland, and areas of natural vegetation cover). Trace elements clearly out-performed water-soluble ions for tracking spatial sources of dust. We passed the thirteen trace elements to stage-two for stepwise discriminant function analysis (DFA). The DFA yielded five trace elements (Fe, Sr, Mn, Cr and Pb) with optimum composite fingerprints that correctly discriminate 87 % of our source samples (Table 2 and Fig. 3).

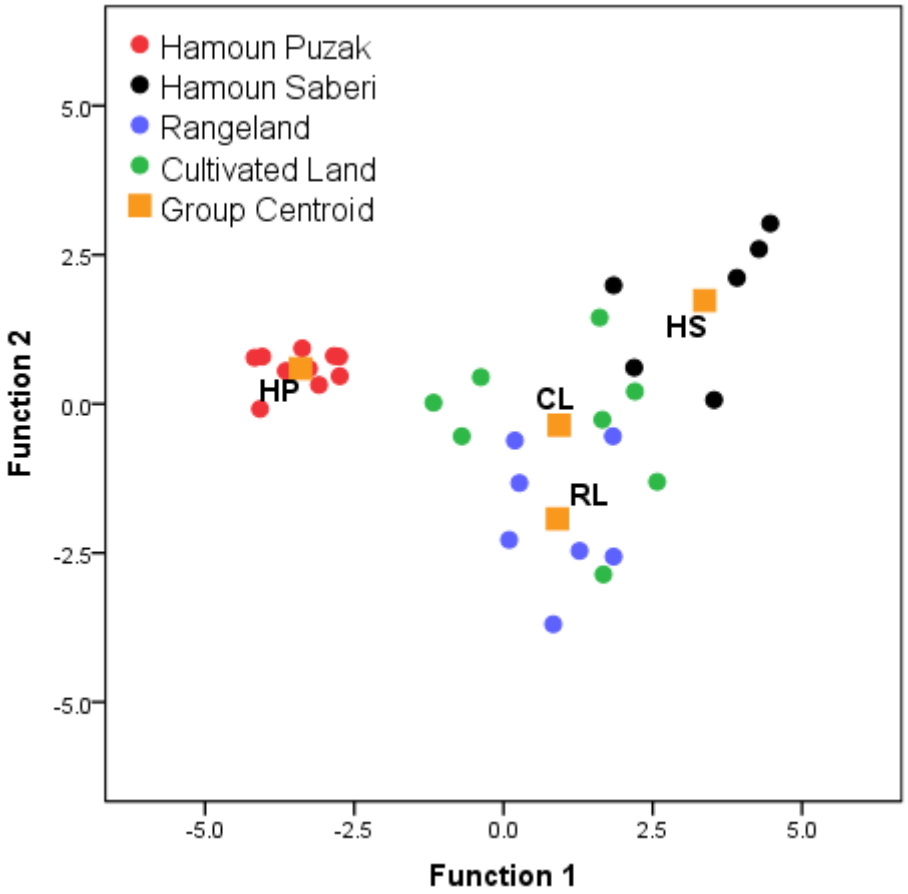

Figure 3. Scatterplot constructed from the first and second functions derived from a stepwise DFA for the source groups including the four land (i.e. Hamoun Puzak (HP), Hamoun Saberi (HS), cultivated land (CL) and uncultivated rangeland (RL). Five optimum fingerprints (Fe, Sr, Mn, Cr and Pb) were used to construct the scatterplot and 87% of the source samples are discriminated, correctly.

4.2 Using GLUE to constrain uncertainty in the source contributions of dust

Uncertainty intervals of source contributions estimated by our GLUE-mixing model at the 95 % confidence level are presented in Figure 4. These results show that the most important dust source is clearly Hamoun Puzak (FigS 4a and 5). Median contributions from this lake-bed span 29 to 88 % (samples 33 and 45, respectively). Hamoun Saberi is a less important source for our samples. Median contributions from this lake bed span 3 to 24 % (samples 11 and 33, respectively) (Figs. 4b). The sparsely vegetated rangeland is the least active dust source. Median contributions span 2 to 22 % (samples 45 and 34, respectively) (Fig. 4c). Cultivated farmland is recognized as the second-most important source for all of 57 samples. Median contributions from farmland span 4 to 25 % (samples 23 and 34, respectively) (Figs. 4d). We note that for most samples, the lower-limit of predicted uncertainty is zero for contributions from the three sources other than Hamoun Puzak (Figs. 4b-d).

Figure. 5 presents an overview of the source contributions with all samples plotted together as a frequency histogram.

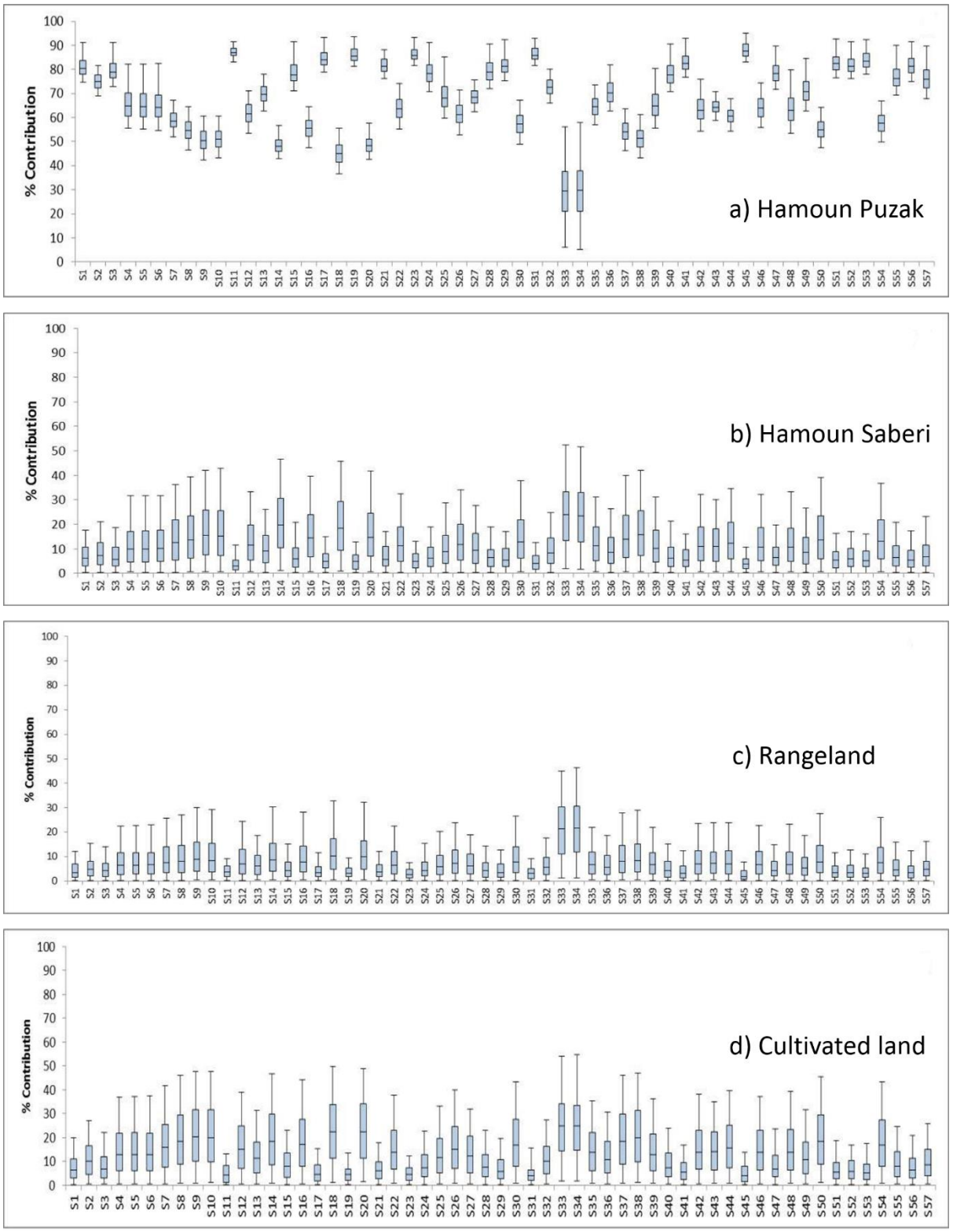

Figure 4. GULE results for dust source contributions yielding 95% confidence limits (with percentiles 2.5, 25, 50, 75 and 97.5). A) Hamoun Puzak; B) Hamoun Saberi; C) uncultivated rangeland; and d) cultivated land.

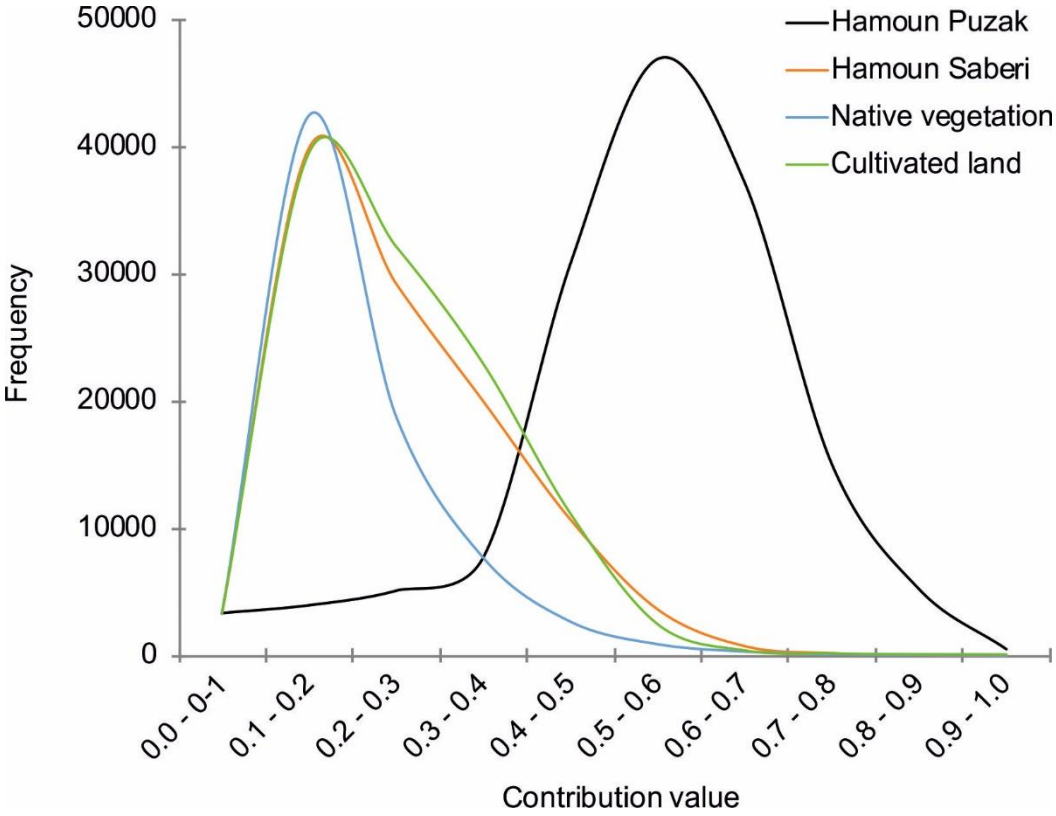

Figure 5. Summary of all source contributions plotted as a probability density function.

5. Discussion

Sediment fingerprinting is a highly effective technique for quantifying source contributions of fluvial sediments (e.g. Collins et al., 1997; Walling, 2005; Stone et al., 2014; Zhou et al., 2016a; Manjoro et al., 2017) and aeolian sands (e.g. Liu et al., 2016; Gholami et al., 2017a,b). Here we build upon this approach by exploring the potential of the GLUE methodology for distinguishing spatially proxima aeolian dust sources with similar underlying geology and geomorphology. We demonstrate its efficacy at formally quantifying the uncertainty distributions associated with aeolian dust fingerprinting due to spatial and temporal variation in the dust cycle, and use the method to reveal spatial complexity - alongside an unexpected lack of temporal complexity - in the nature of the dust sources.

5.1 Environmental context of dust emissions

The strong interannual correlation between dusty days and the surface area of exposed lake floors indicates that i) dust storms in the Sistan-Hamoun region are directly related to the dryness of the Hamoun lakes, and ii) these lake beds are the main source of dust emissions (Goudie and Middleton 2006; Rashki et al., 2012; 2013a; 2013b; 2015). Such relationships are not uncommon, as worldwide observations suggest that exposed dry lake beds can govern the frequency and intensity of dust

storms; for example, at Owens Lake, USA (Reheis et al., 2009), Aral Sea, Uzbekistan (Breckle et al., 2012), Makgadikgadi pan complex; Etosha Pan, southern Africa (Prospero et al., 2002; Mahowald et al., 2003; and Washington et al., 2003); and Lake Eyre, Australia (Baddock et al., 2009).

The frequency and magnitude of dust emissions from the Hamoun Lakes has also been related to annual/decadal scale variations in the surface area of the lakes, which varies dramatically. At its maximum extent, observed following the 1998 spring-melt Hirmand River floods (Rashki et al., 2012a), the Hamoun lake complex forms a single body of water ~4500 km^2 in area. This is comprised of Hamoun Hirmand (~1400 km^2), Hamoun Saberi (~1400 km^2) and Hamoun Puzak (~1700km^2). During more typical lake-full episodes, these bodies of water are not conjoined; for instance, during the spring of 1996 (Figure 6a), Hamoun Saberi spanned ~815km^2 and Hamoun Puzak spanned 375km^2. Hamoun Hirmand lies mostly downwind of Zabol, and hence is not considered further. Between 1999 and 2010 a prolonged drought, likely related to the El Nino Southern Oscillation, resulted in the rapid and sustained desiccation of the Hamoun lakes, with a concomitant increase in the frequency of dusty days (Rashki et al., 2012; 2013). Since 2010, lake levels have been highly variable (Fig. 6), with returns to lake-full conditions experienced around 2011, but a subsequent return to large areas of exposed dry lake beds in recent years.

The implications of such changes can develop rapidly. Within the timeframe of this study (June-October 2014), Hamoun Puzak and Hamoun Saberi lost around 295 km^2 and 640 km^2 of water surface area, respectively (i.e. 98.5% and 99.9% of their extent on June 14th) (Fig. 7). This desiccation affected Hamoun Saberi and Puzak proportionally at very similar rates, but Saberi's larger surface area at the start of this study led to greater absolute change in lake floor exposure area at Saberi. During this period, there was no rainfall recorded at the Zabol meteorological station, but the persistent 'Wind of 120 Days' blew from 327° ± 36° during June-October, with daily average windspeeds up to 35 mph, and 50 of the 138 days of the study period exceeding daily averages of 20 mph.

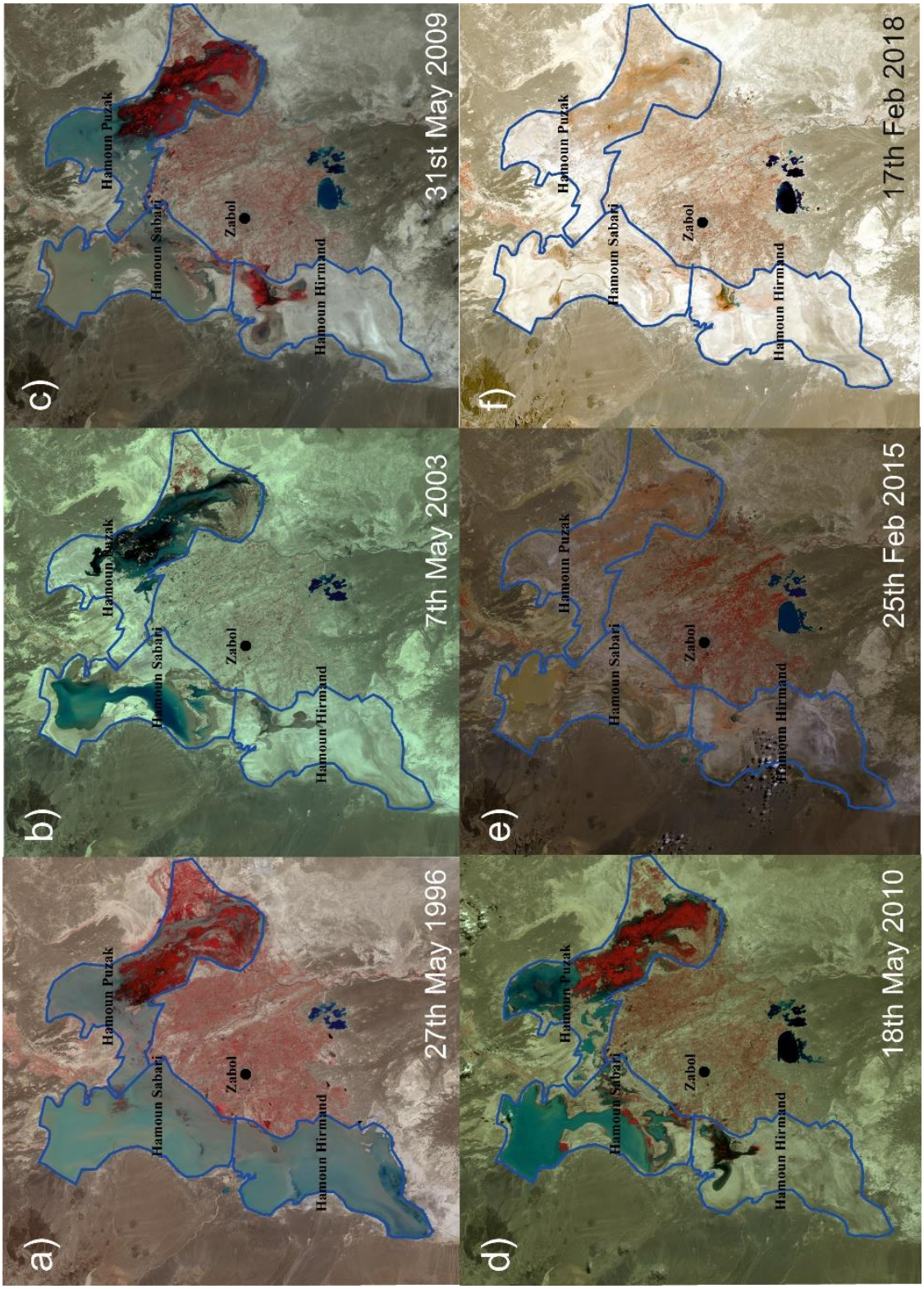

Figure 6. Decadal scale changes in the Hamoun Lakes. Following lake-full conditions in the late 1990s (a), a sustained decade of drought (b and c) resulted in the exposure of large areas of dry lake-beds and therefore potential dust sources. Since then, levels have varied and often changed rapidly (d, e and f). All images are infrared/red/green composites based on Landsat 5 and 8 imagery, using Bands 4/3/2 and 5/4/3 respectively. Vegetation is shown as red tones.

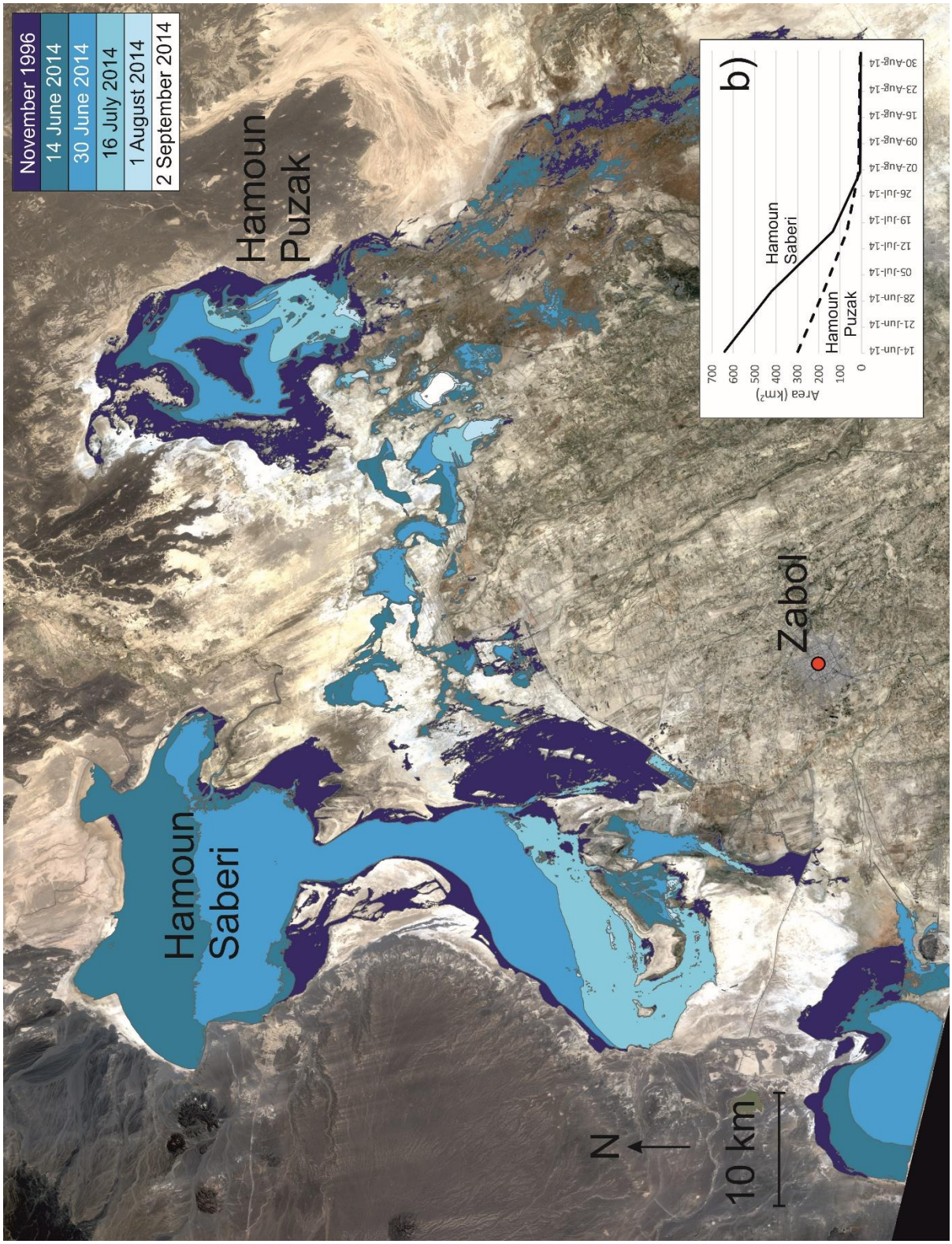

Figure 7. Changes in the surface extent of the Hamoun Lakes between June and September, 2014. Note the rapid desiccation during June and July, and resultant exposure of new surfaces for potential deflation.

5.2. Dust sources: dry beds of Hamoun Lakes

The GLUE results (Figs 4 and 5) reveal that the dominant source of dust collected at Zabol is Hamoun Puzak, and also that in general, the sources of the dust vary little over the three month period from June to the beginning of October, 2014. This finding is unexpected for a number of reasons. Firstly, with the wind at Zabol during this period coming from the northwest to north-northwest (327° ± 36°), the most obvious candidate source of the Zabol dust is the upwind Hamoun Saberi (Figures. 1 and 7). Yet, consistently, Hamoun Puzak contributes ~40-90% (uncertainties included) of the dust received at Zabol. Furthermore, given the rapid increase in Saberi's exposed dry bed during the early period of sampling, its contribution would be expected to increase proportionally over this period. But Saberi's contributions actually vary little during the season (Fig. 4). When the surface area of the lakes is considered, either relative to lake-full conditions (Figure 8a and 8c), or as absolute surface areas (Figure 8b and 8d), there is little temporal relationship with the relative dust contributions of the two lake beds.

Similarly, investigation of the meteorological conditions during June-October do not readily explain the dominance of Hamoun Puzak. There is no clear correlation with either wind magnitude, or direction, that can readily explain the dominance of Puzak, and no obvious explanation arise for the occasional excursions when other sources contribute markedly more. For instance, on August 27th replicate samples were collected (S33 and S34 in Fig. 4) and yield consistent results- note that, for consistency, only one of these samples is included in Figs. 8 and 9.

These result suggest that Hamoun Puzak – or at least the western margin of Hamoun Puzak, where the source samples were collected (Fig. 1) - is a prolific and persistent source of dust over Zabol irrespective of the existence of large adjacent alternative sources. Why is Hamoun Puzak such an effective dust emitter? And why, despite its size and position directly upwind of Zabol, does Hamoun Saberi contribute relatively little? We propose that several factors may be at play, as follows.

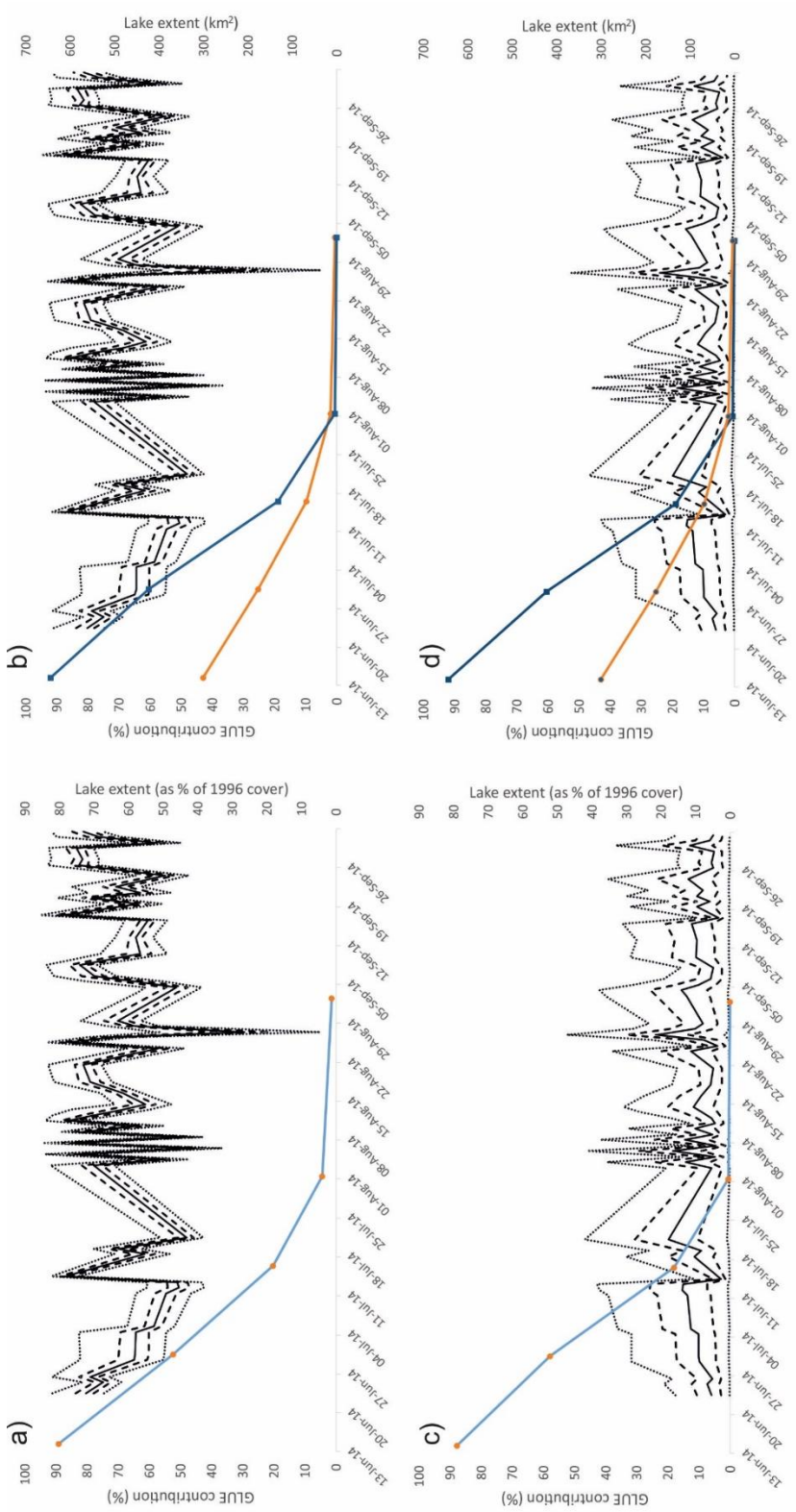

Figure 8. The relative contributions of a) and b) Hamoun Puzak and c) and d) Hamoun Saberi, plotted alongside a) and c) the surface area of the lakes (expressed as a percentage of the 1996 lake-full condtions) and b) and d) the absolute surface area of the lakes. There is no consistent trend in dust provenance, despite the changing area of the potential sources. Solid lines indicate the median estimate, dashed lines the first and third quartiles and dotted lines the 2.5% and 97.5% bounds.

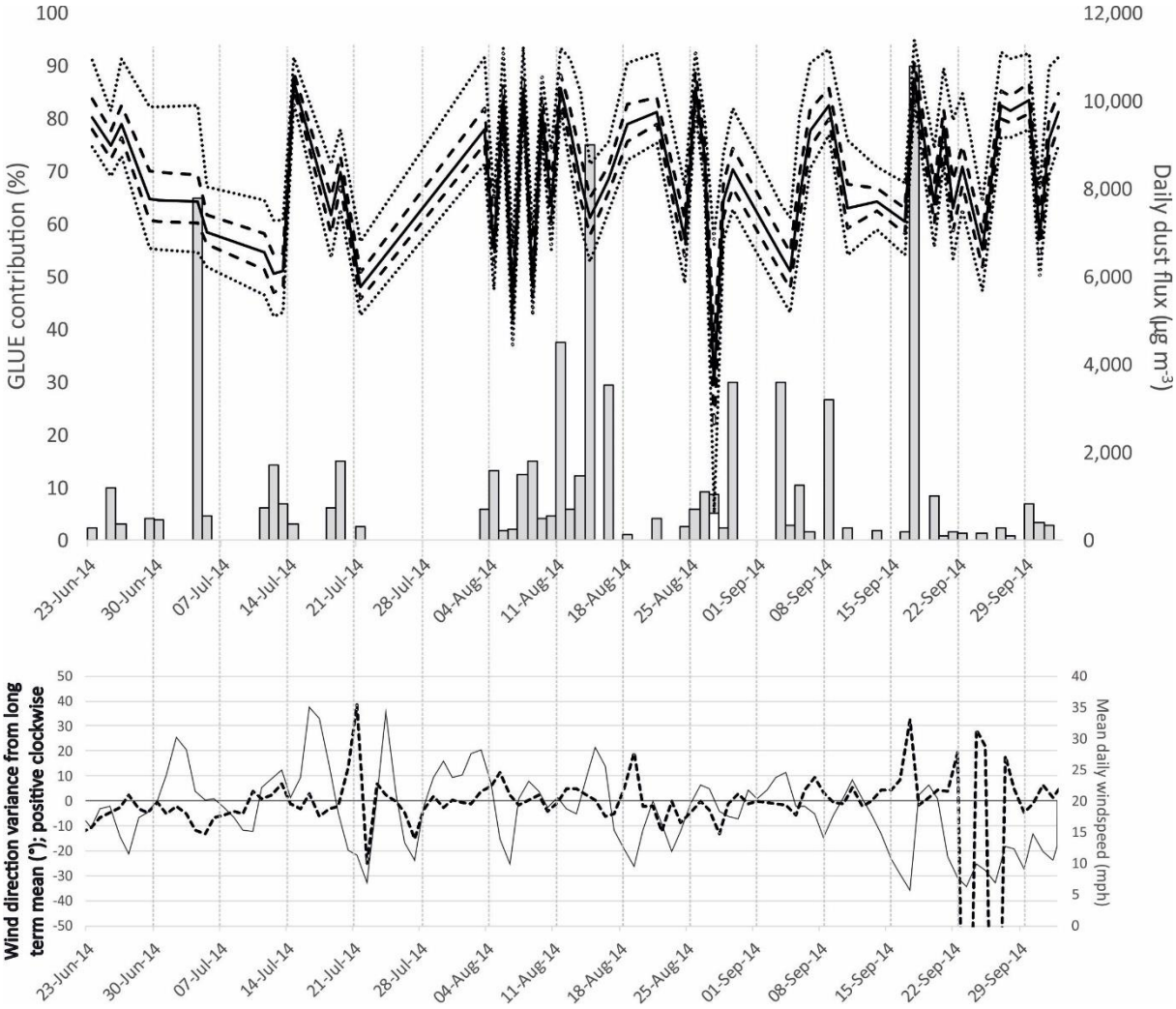

Figure 9. The dominant dust contribution from Hamoun Puzak (top; key for lines as in Figure 8), shown alongside the magnitude of dust collected at Zabol (bars), and the mean daily wind speed (thin solid line) and variance in mean wind direction (bold dashed line).

First, let us consider the hydrological setting and sedimentology of the area. The Hamoun Lakes are predominantly fed with water from the Hirmand River to the east, with the Khash River also feeding directly into Hamoun Puzak from the east. Hamoun Saberi is fed largely from the north by the Harut and Farah rivers. The sampled region at the western margin at Hamoun Puzak lies in series of channels and small closed basins which act as spillways connecting the lakes during lake-full episodes, and thus is likely to have distinctly different sedimentology from lake bed areas subject to direct lacustrine sedimentation (King et al., 2011, Sweeney et al., 2011). Evidence that these sediments are distinct from those of Hamoun Saberi is implicitly provided in the primary function of the DFA used here to define the characteristics of these dusts (Fig. 3). The wind regime necessary for aeolian transport to Zabol from western Hamoun Puzak is compatible with this zone being a dominant source, as northerly orientation lies well within the 327° ± 36° (one sigma) direction of the observed winds. It may also be

that the transport pathways associated with the low-level jet from the north are strongly impacted by topography. We note that wind streaks evident on the satellite imagery of the region suggest that topography is steering and deflecting local winds in a complex manner.

This orientation, however, raises another question: Why does Hamoun Saberi, which lies directly upwind of Zabol, not contribute more to Zabol's dust flux, especially during the latter part of our study when an additional 640 km^2 of dry lake bed became exposed? It is well-reported that dust production can be spatially highly variable, even at sub-basin scales (Mahowald et al., 2003, Reheis et al., 2002, Bullard et al., 2008). One possibility relates to the differing geochemistry of the sediments that can promote the formation of protective crusts. Field experiments have shown that, dry river courses that are replenished frequently with fine-grained fluvial sediment can be much more effective at producing deflatable dust relative to playas and, counter-intuitively, playa centres are relatively low emission sources (Sweeney et al., 2011, King et al., 2011). Dry lake-bed deposits from the Mojave, for instance, have been reported to yield less dust than those with fluctuating water-levels (Reynolds et al., 2007), and the progressive and rapid desiccation of Hamoun Saberi during the study period may have been simply unfavourable for the generation of deflatable dust.

Conversely, it may be that exogenic water supply from the northerly channels sufficiently dampened the surface to limit additional deflation. We note that shallow flooding was observed during the field sample collection, despite the lack of rain observed either in Zabol, or the fortnightly Landsat images. Over longer timescales, rates of aeolian erosion have been shown to inversely relate to soil moisture (Whitney et al., 2015). Although the whole region is sparsely vegetated, the role of vegetation in influencing surface roughness and thus susceptibility to aeolian erosion also cannot be overlooked (e.g. Cowie et al., 2013, Li et al., 2007). Lastly, we point to the cause of the additional 13% of variability, which was not well explained by the discriminant function analysis of the source sediments. This variability may imply that a significant component of Zabol dust derives from outside the immediate area of the Hamoun Lakes. Dust plumes transported from Karakum desert in Turkmenistan may affect the Sistan region (Kaskaoutis et al., 2015) and may be a source of exogenous dust not accounted for among the four potential sources we sampled. In short, further work is needed to identify precisely why Hamoun Puzak dominates the aeolian dust flux at Zabol.

5.3. Dust sources: cultivated and uncultivated land

The connection between land management, agriculture and aeolian dust emissions are well documented (Wiggs and Holmes, 2011, Okin et al., 2001), and the role of agriculture in exacerbating

drought-driven dust events such as the decade-scale 'Dust Bowl' of 1930s USA is clearly established (Worster, 2004). We find that the cultivated cropland to the north of Zabol is the region's second largest overall source of dust (Fig. 4), slightly out-stripping Hamoun Saberi, and contributing substantially more than uncultivated rangeland with sparse vegetation. Desertification (i.e. semi-arid and arid land degradation) has been recognized in other regions of Iran (Sepehr et al., 2007), and given the difficulties of agriculture in such an extremely dry and hot climate, it is unsurprising that sustainable land management is difficult to achieve. The spread of wind erosion is challenging land managers worldwide - from the Argentinian Pampas (Buschiazzo and Zobeck, 2008) to the Tibetan Plateau (Zhang et al., 2012); and even temperate regions such as southern Sweden (Barring et al., 2003). The findings here that cultivation-based farming is the second largest contributor to Zabol's dust flux (with median contributions of 4-25% for individual samples) highlights an anthropogenic dust source that may be quelled through more considered farming practices in the future.

6. Conclusion

Identifying source(s) of aeolian sediments (sand and dust) is essential to improved planning and management of arid and semi-arid regions. Here we present a quantitative sediment fingerprinting approach coupled with the GLUE methodology to quantify source contributions of dust to the city of Zabol in the Sistan-Hamoun region of south-east Iran. Zabol consistently ranks globally as one of the most susceptible to fine (PM2.5 and PM10) aerosol pollutants. Using GLUE, we have assigned quantitative estimates of the relative contributions of four potential dust sources; two dry lake beds (Hamoun Puzak and Hamoun Saberi), cultivated land, and sparsely-vegetated uncultivated rangeland. The dry bed of Hamoun Puzak is the major source supplying sediment for dust samples, with cultivated land contributing more than Hamoun Saberi or uncultivated areas. Robust estimates of uncertainty reveal that whilst the other three dust sources are broadly similar in magnitude, the western end of Hamoun Puzak is undoubtedly the main source.

The samples used for these analyses were collected over a three-month period, during the first half of which the surface water extent of both Puzak and Saberi lakes decreased by > 98%.Yet, the relative contributions from the different land classes remained remarkably consistent. We also note that despite a persistent seasonal wind bearing NW-NNW upon Zabol, the main dust source lies to the northerly segment of the winds observed. This suggests that either the median wind direction is not the most dust-bearing, or the transport pathways are more complex than suspected.

Our results demonstrate both the potential and the necessity of combining quantitative provenancing techniques with robust uncertainty methods and, ultimately, improved land management. The straightforward approach of linking the main wind direction to a large and rapidly-drying lake bed (Hamoun Saberi) does not yield a good outcome, in this case. Spatial variation in dust sources has been identified elsewhere, most strikingly at the Bodélé Depression in the Chadian Sahara (Washington et al., 2003); here we demonstrate the application of methods with the scope to identify such spatial variation from the point of receipt of the dust. We are unable to outline the exact reasons for Hamoun Puzak's susceptibility to aeolian erosion. However, we attribute notable influence to the geomorphological conditions of the western arm of the Puzak, with its array of interconnected small basins and spillways proving more prone to generating dusts emissions.

REFERENCES

Aaron, S. M., Blakowski, M. A., Aciego, S. M., Stevenson, E. I., Sims, K. W. W., Scott, S, R., and Aarons, C. (2017). Geochemical characterization of critical dust source regions in the American West. Geochimica et Cosmochimica Acta 215; 141-161. http://dx.doi.org/10.1016/j.gca.2017.07.024

Abban, B., Papanicolaou, A, N., Cowles, M. K., Wilson, C. G., Abaci, O., Wacha, K., Schilling, and K., Schnobelen, D. (2016). An enhanced Bayesian fingerprinting framework for studying sediment source dynamics in intensively managed landscapes. Water Resource Research, 52, 4646-4673. doi:10.1002/2015WR018030.

Alizadeh Choobari, O., Zawar-Reza, P., and Sturman, A. (2014). The "wind of 120 days" and dust storm activity over the Sistan Basin. Atmospheric Research, 143; 328-341. http://dx.doi.org/10.1016/j.atmosres.2014.02.001

Baddock, M. C., Bullard, J. E., and Bryant, R. G (2009). Dust source identification using MODIS: a comparison of techniques applied to the Lake Eyre Basin, Australia. Remote Sens Environ, 113:1511–28.

Barring, L., Jonsson, P., Mattsson, J. O. & Ahman, R. 2003. Wind erosion on arable land in Scania, Sweden and the relation to the wind climate - a review. *Catena,* 52**,** 173-190.

Beven, K. and Binley, A. (1992). The future of distributed models: Model calibration and uncertainty prediction. Hydrological Processes, 6(3), 279-298. doi: 10.1002/hyp.3360060305.

Breckle, S.W., Wucherer, W., Liliya, A., Dimeyeva, L. A., Nathalia, P., and Ogar, N.P. (2012). Aralkum - a man-made desert: the desiccated floor of the Aral Sea (Central Asia). Springer; 2012486.

Bullard, J., Baddock, M., Mctainsh, G. & Leys, J. 2008. Sub-basin scale dust source geomorphology detected using MODIS. *Geophysical Research Letters,* 35.

Buschiazzo, D. E. & Zobeck, T. M. 2008. Validation of WEQ, RWEQ and WEPS wind erosion for different arable land management systems in the Argentinean Pampas. *Earth Surface Processes and Landforms,* 33**,** 1839-1850.

Cao, H., Amiraslani, F., Liu, J., and Zhou, N. (2015). Identification of dust storm source areas in West Asia using multiple environmental datasets. Science of the Total Environment, 502; 224-235. http://dx.doi.org/10.1016/j.scitotenv.2014.09.025

Cao, J. J., Zhu, C. S., Chow, J. C., Liu, W. G., Han, Y. M., and Watson, J. G. (2008). Stable carbon and oxygen isotopic composition of carbonate in fugitive dust in the Chinese Loess Plateau. Atmospheric Environment, 42; 9118-9122. doi:10.1016/j.atmosenv.2008.09.043

Chavagnac, V., Lair, M., Milton, J. A., Lioyd, A., Croudace, I .W., Palmer, M. R., Green, D. R. H., and Cherkashev, G. A. (2008). Tracing dust input to the Mid-Atlantic Ridge between 14°45'N and 36°14'N: Geochemical and Sr isotope study. Marine Geology, 247; 208-225. doi:10.1016/j.margeo.2007.09.003

Chen, J., Li, G., Yang, J., Rao, W., Lu, H., Balsam, W., Sun, Y., and Ji, J. Nd and Sr isotopic characteristics of Chinese deserts: Implications for the provenances of Asian dust. Geochimica et Cosmochimica Acta, 71; 3904-3914.

Cherboudj, I., Beegum, S. N., and Ghedira, H. (2016). Identifying natural dust source regions over the Middle-East and North-Africa: Estimation of dust emission potential. Earth Science Review. http://dx.doi.org/10.1016/j.earscirev.2016.12.010

Collins, A. L., and Walling, D. E. (2007). Sources of fine sediment recovered from the channel bed of lowland groundwater-fed catchments in the UK. Geomorphology, 88, 120–138. doi:10.1016/j.geomorph.2006.10.018

Collins, A.L., Walling, D.E., and Leeks, G.J.L. (1997). Fingerprinting the origin of fluvial suspended sediment in larger river basins: combining assessment of spatial provenance and source type. Geografiska Annaler, 79, 239–254.

Collins, A.L., Zhang, Y., Walling, D.E., Grenfell, S.E., Smith, P., Grischeff, J., … Brogden, D. (2012). Quantifying fine-grained sediment sources in the River Axe Catchment, southwest England: Application of a Monte-Carlo numerical modelling framework incorporating local and genetic algorithm optimisation. Hydrological Processes, 26 (13), 1962–1983. doi:10.1002/hyp.8283.

Cooper, R. J., Krueger, T., Hiscock, K. M., & Rawlins, B. G. (2014). Sensitivity of fluvial sediment source apportionment to mixing model assumptions : A Bayesian model comparison. Water Resources Research, 9031–9047. doi:10.1002/2014WR016194.

Cooper, R. J., Krueger, T., Hiscock, K. M., & Rawlins, B. G. (2015). High-temporal resolution fluvial

sediment source fingerprinting with uncertainty: A Bayesian approach. Earth Surface Processes and Landforms, 40(1), 78–92. doi:10.1002/esp.3621

Cowie, S. M., Knippertz, P. & Marsham, J. H. 2013. Are vegetation-related roughness changes the cause of the recent decrease in dust emission from the Sahel? *Geophysical Research Letters,* 40**,** 1868-1872.

Dahmardeh Behrooz, R., Esmaili-Sari, A., Bahramifar, N., and Kaskaoutis, D. G. (2017a). Analysis of the TSP, PM10 concentrations and water-soluble ionic species in airborne samples over Sistan, Iran during the summer dusty period. Atmospheric Pollution Research, 8; 403-417. http://dx.doi.org/10.1016/j.apr.2016.11.001

Dahmardeh Behrooz, R., Esmaili-Sari, A., Bahramifar, N., and Kaskaoutis, D. G., Saeb, K., and Rajaei, F. (2017b). Trace-element concentrations and water-soluble ions in size-segregated dust-borne and soil samples in Sistan, southeast Iran. Aeolian Research, 25; 87-105. http://dx.doi.org/10.1016/j.aeolia.2017.04.001

Del Rio-Salas, R., Ruiz, J., De la O-Villanueva, M., Valencia-Moreno, M., Moreno,-Rodriguez, V., Gomez-Alvarez, A., Grijalva, T., Mendivil, H., Paz-Moreno, F., and Meza-Figueroa, D. (2012). Tracing geogenic and anthropogenic sources in urban dusts: Insights from lead isotopes. Atmospheric Environment, 60; 202-210. http://dx.doi.org/10.1016/j.atmosenv.2012.06.061

Esmaeili, A. and Omrani, M. (2007). Efficiency analysis of fishery in Hamoon lake using DEA approach. J. Appl. Sci, 7; 2856-2860.

Ge, Y., Abuduwaili, J., Ma, L., Wu, N., and Liu, D. (2016). Potential transport pathways of dust emanating from the playa of Ebinur Lake, Xinjiang, in arid northwest China. Atmospheric Research, 178-179; 196-206. http://dx.doi.org/10.1016/j.atmosres.2016.04.002

Gholami, H., Middleton, N., Nzari Samani, A., and Wasson, R. (2017a). Determining contribution of sand dune potential sources using radionuclides, trace and major elements in central Iran. Arab J Geosci, 10:163. doi. 10.1007/s12517-017-2917-0.

Gholami, H., Telfer, M. W., Blake, W. H., and Fathabadi, A. (2017) Aeolian sediment fingerprinting using a Bayesian mixing model. Earth Surf. Process. Landforms, 42: 2365–2376. doi: 10.1002/esp.4189.

Gong, Y., Shen, Zh, Hong, Q., Liu, R., and Liao, Q. (2011). Parameter uncertainty analysis in watershed total phosphorus modeling using the GLUE methodology. Agriculture, Ecosystems and Environment 142; 246-255. doi:10.1016/j.agee.2011.05.015

Goossens, D. (2003). On-site and off-site effects of wind erosion. In: Warren A (ed) Wind erosion on agricultural land in Europe. European Commission, Luxembourg, pp. 29–38

Goudie, A. S. and Middleton, N. J. (2006). Desert dust in the global system. Springer.

Grousset, F. E. and Biscaye, P. E. (2005). Tracing dust sources and transport patterns using Sr, Nd and Pb isotopes. Chemical Geology, 222; 149-167. doi:10.1016/j.chemgeo.2005.05.006

Hamidi, M., Kavianpour, M. R., and Shao, Y. (2014). Numerical simulation of dust events in the Middle East. Aeolian Research, 13; 59-70. http://dx.doi.org/10.1016/j.aeolia.2014.02.002

Hassan, A. E., Bekhit, H. M., and Chapman, J. B. (2008). Uncertainty assessment of a stochastic groundwater flow model using GLUE analysis. Journal of Hydrology, 362; 89-109. doi:10.1016/j.jhydrol.2008.08.017

Kaskaoutis, D.G., Rashki, A., Francois, P., Dumka, U.C., Houssos, E.E., and Legrand, M. (2015). Meteorological regimes modulating dust outbreaks in southwest Asia: the role of pressure anomaly and Inter-Tropical Convergence Zone on the 1–3 July 2014 case. Aeolian Research. 18, 83–97.

Kaskaoutis, D.G., Rashki, A., Houssos, E. E., Goto, D., and Nastos, P. T. (20[illegible] Extremely high aerosol loading over Arabian Sea during June 2008: the specific role of the atmospheric dynamics and Sistan dust storms. Atmospheric Environment. Doi: 10.1016/j.atmosenv.2014.05.012

King, J., Etyemezian, V., Sweeney, M., Buck, B. J. & Nikolich, G. 2011. Dust emission variability at the Salton Sea, California, USA. *Aeolian Research,* 3**,** 67-79.

Krom, M.D., Cliff, R. A., Eijsink, L. M., Herut, B., and Chester, R. (1999). The characterisation of Saharan dusts and Nile particulate matter in surface sediments from the Levantine basin using Sr isotopes. Marine Geology, 155; 319-330.

Li, J., Okin, G. S., Alvarez, L. & Epstein, H. 2007. Quantitative effects of vegetation cover on wind erosion and soil nutrient loss in a desert grassland of southern New Mexico, USA. *Biogeochemistry,* 85**,** 317-332.

Liu, B., Niu, Q., Qu, J., and Zu, R. (2016). Quantifying the provenance of aeolian sediments using multiple composite fingerprints. Aeolian Research, 22, 117-122. dx.doi.org/10.1016/j.aeolia.2016.08.002

Long, X., Li., N., Tie, X., Cao, J., Zhao, Sh., Huang, R., Zhao, M., Li, G., and Feng, Tian. (2016). Urban dust in the Guanzhong Basin of China, part I: A regional distribution of dust sources retrieved using satellite data. Science of the Toatal Environment, 541; 1603-1613. http://dx.doi.org/10.1016/j.scitotenv.2015.10.063

Mahowald, N. M., Bryant, R. G., del Corral., J., and Steinberger, L. (2002). Ephemeral lakes and desert dust sources. Geophys Res Lett, 30:1074. http://dx.doi.org/10.1029/2002GL016041

Manjoro, M., Rowntree, K., Kakembo, V., Foster, I., and Collins, A. L. (2016) [illegible]e of sediment source fingerprintin g to assess the role of subsurface erosion in the supply of fine sediment in a

degraded catchment in the Eastern Cape, South Africa. Journal of Environmental Management, xxx, 1-15. dx.doi.org/10.1016/j.jenvman.2016.07.019

Massoudieh, A., Gellis, A., Banks, W. S., & Wieczorek, M. E. (2013). Suspended sediment source apportionment in Chesapeake Bay watershed using Bayesian chemical mass balance receptor modeling. Hydrological Processes, 27(24), 3363–3374. doi:10.1002/hyp.9429

Middleton NJ. (1986). Dust storms in the Middle East. J Arid Environ,10:83–96

Moghaddamnia, A., Ghafari, M.B., Piri, J., Amin, S., and Han, D. (2009). Evaporation estimation using artificial neural networks and adaptive neuro-fuzzy inference system techniques. Adv. Water Resour. 32, 88–97

Montovan, P. and Todini, E. (2006). Hydrological forecasting uncertainty assessment: Incoherence of the GLUE methodology. Journal of Hydrology, 330; 368-381. doi:10.1016/j.jhydrol.2006.04.046

Motha, J.A., Wallbrink, P.J., Hairsine, P.B., and Grayson, R.B. (2003). Determining the sources of suspended sediment in a forested catchment in southeastern Australia. Water Resources, 39 (3), 1056. doi:10.1029/2001wr000794.

Nabavi, S. O., Haimberger, L., and Samimi, C. (2016). Climatology of dust distribution over West Asia from homogenized remote sensing data. Aeolian Research, 21; 93-107. http://dx.doi.org/10.1016/j.aeolia.2016.04.002

Nabavi, S. O., Haimberger, L., and Samimi, C. (2017). Sensitivity of WRF-chem predictions to dust source function specification in West Asia. Aeolian Research, 24; 115-131. http://dx.doi.org/10.1016/j.aeolia.2016.12.005

Nakano, T., Yokoo, Y., Nishikawa, M., and Koyanagi, H. (2004). Regional Sr–Ndisotopic ratios of soil minerals in northern China as Asian dust fingerprints. Atmospheric Environment, 38; 3061-3067. doi:10.1016/j.atmosenv.2004.02.016

Okin, G. S., Murray, B. & Schlesinger, W. H. 2001. Degradation of sandy arid shrubland environments: observations, process modelling, and management implications. *Journal of Arid Environments,* 47**,** 123-144.

Rashki, A., Arjmand, A., and Kaskaoutis, D. G. (2017). Assessment of dust activity and dust-plume pathways over Jazmurian Basin, southeast Iran. Aeolian Research, 24; 145-160. http://dx.doi.org/10.1016/j.aeolia.2017.01.002

Rashki, A., Eriksson, P. G., Rautenbach, C. J. D., Kaskaoutis, D. G., Grote, W., and Dykstra, J. (2013a). Assessment of chemical and mineralogical characteristics of airborne dust in the Sistan region, Iran. Aeolian Research, 90; 227-236. http://dx.doi.org/10.1016/j.chemosphere.2012.06.059

Rashki, A., Kaskaoutis, D. G., Francois, P., Kosmopoulos, P. G., and Legrand, M. (2015). Dust-storm dynamics over Sistan region, Iran: Seasonality, transport characteristics and affected areas. Aeolian Research, 16; 35-48.

Rashki, A., Kaskaoutis, D. G., Goudie, A. S., and Kahn, R. A. (2013b). Dryness of ephemeral lakes and consequences for dust activity: The case of the Hamoun drainage basin, southeastern Iran. Science of the Total Environment, 463-464; 552-564. http://dx.doi.org/10.1016/j.scitotenv.2013.06.045

Rashki, A., Kaskaoutis, D. G., Rautenbach, C. J. D., Eriksson, P. G. (2012a). Changes of Permanent Lake Surfaces, and Their Consequences for Dust Aerosols and Air Quality: The Hamoun Lakes of the Sistan Area, Iran. In: Hayder Abdul-Razzak (Eds.), Atmospheric Aerosols - Regional Characteristics. DOI: 10.5772/48776

Rashki, A., Kaskaoutis, D. G., Rautenbach, C. J. D., Eriksson, P. G., Qiang, M., and Gupta, P. (2012b). Dust storms and their horizontal dust loading in the Sistan region, Iran. Aeolian Research, 5; 51-62. doi:10.1016/j.aeolia.2011.12.001

Reheis, M. C., Budahn, J. R. & Lamothe, P. J. 2002. Geochemical evidence for diversity of dust sources in the southwestern United States. *Geochimica Et Cosmochimica Acta,* 66**,** 1569-1587.

Reheis, M., Budahn, J. R., Lamothe, P. J., and Reynolds, R. L. (2009). Compositions of modern dust and surface sediments in the Desert Southwest United States. J Geophys Res, 114: F01028. http://dx.doi.org/10.1029/2008JF001009

Reynolds, R.L., Yount, J.C., Reheis, M., Goldstein, H, Chavez Jr, P., Fulton, R, Whitney, J., Fuller, C., Forester, R.M. (2007). Dust emission from wet and dry playas in the Mojave Desert, USA. Earth Surface Processes and Landforms, 3; 1811-1827. https://doi.org/10.1002/esp.1515

Rezazadeh, M., Irannejad, P., and Shao, Y. (2013). Climatology of the Middle East dust events. Aeolian Research, 10; 103-109. http://dx.doi.org/10.1016/j.aeolia.2013.04.001

Schepanski, K., Tegen, I., and Macke. A. (2012). Comparison of satellite based observations of Saharan dust source areas. Remote Sensing of Environment, 123; 90-97. doi:10.1016/j.rse.2012.03.019

Sepehr, A., Hassanli, A. M., Ekhtesasi, M. R. & Jamali, J. B. 2007. Quantitative assessment of desertification in south of Iran using MEDALUS method. *Environmental Monitoring and Assessment,* 134**,** 243.

Shen, Z., Caquineau, S., Cao, J., Zhang, X., Han, Y., Gaudichet, A., and Gomes, L. (2009). Mineralogical characteristics of soil dust from source regions in northern China. Particulogy, 7; 507-512. doi:10.1016/j.partic.2009.10.001

Sherriff, S. C., Franks, S. W., Rowan, J. S., Fenton, O., & Ó'hUallacháin, D. (2015). Uncertainty-based assessment of tracer selection, tracer non-conservativeness and multiple solutions in sediment fingerprinting using synthetic and field data. Journal of Soils and Sediments, 15(10), 2101–2116. doi:10.1007/s11368-015-1123-5

Smith, H.G., and Blake, W.H. (2014). Sediment fingerprinting in agricultural catchments: A critical re-examination of source discrimination and data corrections. Geomorphology, 204, 177–191. doi:10.1016/j.geomorph.2013.08.003.

Stewart, H. A., Massoudieh, A., & Gellis, A. (2015). Sediment source apportionment in Laurel Hill Creek, PA, using Bayesian chemical mass balance and isotope fingerprinting. Hydrological Processes, 29(11), 2545–2560. doi:10.1002/hyp.10364

Stone, M., Collins, A.L., Silins, U., Emelko, M.B., and Zhang, Y.S. (2014). The use of composite fingerprints to quantify sediment sources in a wildfire impacted landscape, Alberta, Canada. Science of the Total Environment, 473-474, 642–650. doi:10.1016/j.scitotenv.2013.12.052.

Sweeney, M. R., Mcdonald, E. V. & Etyemezian, V. 2011. Quantifying dust emissions from desert landforms, eastern Mojave Desert, USA. *Geomorphology,* 135**,** 21-34.

Sweeney, M. R., Zlotnik, V. A., Joeckel, R. M. & Stout, J. E. 2016. Geomorphic and hydrologic controls of dust emissions during drought from Yellow Lake playa, West Texas, USA. *Journal of Arid Environments,* 133**,** 37-46.

United Nations Environment Programme (UNEP) (2006). History of environmental change in the Sistan basin based on satellite image analysis: 1976–2005; 200660.

Vale, S. S., Fuller, I. C., Procter, J. N., Basher, L. R., and Smith, I. E. (2016). Characterization and quantification of suspended sediment sources to the Manawatu River, New Zealand. Science of the Total Environment, 543, 171–186. doi:10.1016/j.scitotenv.2015.11.003

Viola, F., Noto, L. V., Cannarozzo, G., and Loggia, G. L. (2009). Daily streamflow prediction with uncertainty in ephemeral catchments using the GLUE methodology. Physics and Chemistry of the Earth 34; 701-706.

Voli, M.T., Wegmann, K.W., Bohnenstiehl, D.R., Leithold, E., Osburn, C.L., and Polyakov, V. (2013). Fingerprinting the sources of suspended sediment delivery to a large municipal drinking water reservoir: Falls Lake, Neuse River, North Carolina, USA. Journal of Soils and Sediments, 13 (10), 1692–1707. doi:10.1007/s11368-013-0758-3.

Walling, D.E. (2005). Tracing suspended sediment sources in catchments and river systems. Science of the Total Environment, 344 (1-3), 159–184. doi:10.1016/j.scitotenv.2005.02.011.

Walling, D.E. (2013). The evolution of sediment source fingerprinting investigations in fluvial systems. Journal of Soils and Sediments, 13 (10), 1658–1675. doi:10.1007/s11368-013-0767-

2.

Wang, Y. Q., Zhang. X. Y., Arimoto, R., Cao, J. J., and Shen, Z. X. (2005). Characteristics of carbonate content and carbon and oxygen isotopic composition of northern China soil and dust aerosol and its application to tracing dust sources. Atmospheric Environment, 39; 2631-2642. doi:10.1016/j.atmosenv.2005.01.015

Washington, R., Todd, M., Middleton, N.J., and Goudie, A. S. (2003). Dust storm source areas determined by the Total Ozone Monitoring Spectrometer and surface observations. Ann Assoc Am Geogr, 93: 297–313.

Wei, T., Dong, Z., Kang, Sh., Qin, X., and Guo, Zh. (2017). Geochemical evidence for sources of surface dust deposited on the Laohugou glacier, Qilian Mountains. Applied Geochemistry; 79; 1-8. http://dx.doi.org/10.1016/j.apgeochem.2017.01.024

Whitney, J. W., Breit, G. N., Buckingham, S. E., Reynolds, R. L., Bogle, R. C., Luo, L., Goldstein, H. L. & Vogel, J. M. 2015. Aeolian responses to climate variability during the past century on Mesquite Lake Playa, Mojave Desert. *Geomorphology,* 230**,** 13-25.

Wiggs, G. & Holmes, P. 2011. Dynamic controls on wind erosion and dust generation on west-central Free State agricultural land, South Africa. *Earth Surface Processes and Landforms,* 36**,** 827-838.

World Health Organisation (2016). WHO Global Urban Ambient Air Pollution Database. URL: http://www.who.int/phe/health_topics/outdoorair/databases/cities/en/ (Accessed 23/06/2018).

Worster, D. 2004. *Dust bowl: the southern plains in the 1930s*, Oxford University Press.

Xu, H. (2006). Modification of normalised difference water index (NDWI) to enhance open water features in remotely sensed imagery. International Journal of Remote Sensing, 27; 3025–3033. doi: 10.1080/01431160600589179

Yan, Y., Sun, Y., Ma., L., and Long, X. (2015). A multidisciplinary approach to trace Asian dust storms from source to sink. Atmospheric Environment, 105; 43-52. http://dx.doi.org/10.1016/j.atmosenv.2015.01.039

Yang, J., Li, G., Rao, W., and Ji, J. (2009). Isotopic evidences for provenance of East Asian Dust. Atmospheric Environment, 43; 4481-4490. doi:10.1016/j.atmosenv.2009.06.035

Zhang, D., Zhou, Z. H., Zhang, B., Du, S. H. & Liu, G. C. 2012. The effects of agricultural management on selected soil properties of the arable soils in Tibet, China. *Catena,* 93**,** 1-8.Prospero, J. M., Ginoux, P., Torres, O., Nicholson, S. E., and Gill, T. E. (2002). Environmental characterization of global sources of atmospheric soil dust identified with the Nimbus 7 total ozone mapping spectrometer absorbing aerosol product. Rev Geophys, 40: 2–31

Zhou, H., Chang, W., and Zhang, L. (2016a). Sediment sources in a small agricultural catchment: A composite fingerprinting approach based on the selection of potential sources. Geomorphology, 266, 11-19. dx.doi.org/10.1016/j.geomorph.2016.05.007

Zhou, R., Li, Y., Lu, D., Liu, H., and Zhou, H. (2016b). An optimization based sampling approach for multiple metrics uncertainty analysis using generalized likelihood uncertainty estimation. Journal of Hydrology, 540; 274-286. http://dx.doi.org/10.1016/j.jhydrol.2016.06.030.

Table 1: Summery characteristics of dust samples collected in Zabol during 21 June to 4 October, 2014.

dust sample no	Sampling date	W V* (m/s)	dust mass (ug/m³)	dust sample no	Sampling date	W V* (m/s)	dust mass (ug/m³)
1	23 June 2014	7.1	270.2	30	24 August 2014	6.5	300.15
2	25 June 2014	8.6	1180.5	31	25 August 2014	9	695.65
3	26 June 2014	6.3	380	32	26 August 2014	10.4	1100.15
4	29 June 2014	8.1	500.6	33	27 August 2014**	9.8	1052
5	30 June 2014	9	458	34	27 August 2014***	9.8	922.39
6	4 July 2014	9.5	7800	35	28 August 2014	8	606.29
7	5 July 2014	8.9	570.2	36	29 August 2014	7.4	271.3
8	11 July 2014	10.3	724	37	3 Sep 2014	10	3594.92
9	12 July 2014	10.5	1700.7	38	4 Sep 2014	11.4	3594.92
10	13 July 2014	10.5	831	39	5 Sep 2014	8.1	339.56
11	14 July 2014	8.9	370.3	40	6 Sep 2014	8.5	1243.88
12	18 July 2014	11.3	740.2	41	8 Sep 2014	6.1	186.21
13	19 July 2014	8.3	1800	42	10 Sep 2014	9.1	3188.85
14	21 July 2014	4.8	320.8	43	13 Sep 2014	7.4	296.8
15	3 August 2014	12.3	715.3	44	16 Sep 2014	4.6	213.77
16	4 August 2014	10	1600	45	17 Sep 2014	4.3	192.4
17	5 August 2014	5.1	216	46	19 Sep 2014	10.1	10785.5
18	6 August 2014	6.6	246.4	47	20 Sep 2014	8.5	1013.43
19	7 August 2014	10	1500	48	21 Sep 2014	4.9	111.76
20	8 August 2014	10	1803	49	22 Sep 2014	2.8	179.61
21	9 August 2014	10	480.04	50	24 Sep 2014	3.4	155.98
22	10 August 2014	8	560.04	51	26 Sep 2014	2.3	165.52
23	11 August 2014	9.1	4500	52	27 Sep 2014	5.5	274.83
24	12 August 2014	8.3	720	53	29 Sep 2014	4	90.31
25	13 August 2014	8.3	1480	54	30 Sep 2014	7.1	814.46
26	14 August 2014	11.5	9004.58	55	1 Oct 2014	5.1	413.15
27	16 August 2014	10.9	3529.4	56	2 Oct 2014	5.3	331.67
28	18 August 2014	5.1	126.74	57	3 Oct 2014	7.5	597.6
29	21 August 2014	8.3	498.5				

* W V indicates Wind Velocity; ** Sample collected on the day; *** Sample collected on the night.

Table 2: Results of a two-stage statistical process for selecting optimum composite fingerprints for distinguishing sources of dust.

Kruskal-Wallis H test			Stepwise DFA		
Fingerprint property	Chi-Square	P-value	Step	Entered fingerprint	Wilk's lambda
Trace elements			1	Fe	0.356
Au	6.79	0.079	2	Sr	0.188
Pt	1.58	0.664	3	Mn	0.081
Mg	20.83	0.000**	4	Cr	0.053
Al	1.48	0.686	5	Pb	0.033
Sr	20.6	0.000**			
Li	22	0.000**	*Statistically significant at P<0.05		
Fe	20.9	0.000**	** Statistically significant at P<0.01		
Cr	19.5	0.000**			
Cu	19.5	0.000**			
Zn	5.16	0.16			
As	9.9	0.019*			
Ni	20.75	0.000**			
Pb	9.58	0.022*			
Mn	20.24	0.000**			
Co	18.73	0.000**			
Sn	12.9	0.005**			
Ions					
Na^+	7.24	0.065			
NH^+_4	2.6	0.456			
K^+	4	0.254			
Cl^-	0.4	0.941			
NO^-_2	3.3	0.358			
NO^-_3	7.01	0.072			
Mg^{2+}	1.38	0.709			
Ca^+	14.5	0.002**			

706

Using GLUE to pull apart the provenance of atmospheric dust

Reza Dahmardeh Behrooz[1], Hamid Gholami[2*], Matt W. Telfer[3*], John D. Jansen[4*], Abolhassan Fathabadi[5]

1. Department of Environmental Sciences, Faculty of Natural Resources, University of Zabol, Zabol, Sistan, Iran
2. Department of Natural Resources Engineering, University of Hormozgan, Bandar-Abbas, Hormozgan, Iran.
3. School of Geography, Earth and Environmental Sciences, Plymouth University, Plymouth, Devon PL4 8AA, UK
4. Department of Geoscience, Aarhus University, Aarhus, 8000, Denmark.
5. Department of Range and Watershed Management, University of Gonbad-e-Kavoos, Gonbad-e-Kavoos, Golestan, Iran

Corresponding Authors: Hamid Gholami, hgholami@hormozgan.ac.ir; Matt W Telfer, matt.telfer@plymouth.ac.uk; John Jansen, jdj@geo.au.dk

HIGHLIGHTS

- The GLUE model is applied to reveal the provenance of aeolian dust in Zabol, Iran.
- Quantitative estimates and uncertainties of four different dust sources are discriminated.
- One dry lake, Hamoun Puzak, is by far the dominant dust source, despite others nearby.
- The major dust source is insensitive to large changes in exposed local dry lake beds.
- Cultivated land is the second most important dust source, ahead of some playas.

Using GLUE to pull apart the provenance of atmospheric dust

HIGHLIGHTS

- The GLUE model is applied to reveal the provenance of aeolian dust in Zabol, Iran.
- Quantitative estimates and uncertainties of four different dust sources are discriminated.
- One dry lake, Hamoun Puzak, is by far the dominant dust source, despite others nearby.
- The major dust source is insensitive to large changes in exposed local dry lake beds.
- Cultivated land is the second most important dust source, ahead of some playas.

Abstract

Identifying the sources of aeolian dust is a crucial step in mitigating the associated hazards. We apply a Generalized Likelihood Uncertainty Estimation (GLUE) model to constrain the uncertainties associated with sediment fingerprinting of atmospheric dust in the Sistan region on the Iran-Afghanistan border, one of the world's dustiest places. 57 dust samples were collected from the rooftop of the Zabol Department of Environmental Protection during a summer dusty period from June to October 2014, in addition to 31 surface soil samples collected from potential sources nearby, including cultivated land (n=8), uncultivated rangeland (n=7), and two dry lakes: Hamoun Puzak (n=10) and Hamoun Saberi (n=6). Dust and soil samples were analyzed for 24 tracers including 16 geochemical elements and 8 water-soluble ions. Five optimum composite fingerprints (Fe, Sr, Mn, Cr and Pb) were selected for discriminating sources by a two-stage statistical process involving a Kruskal-Wallis test and stepwise discriminant function analysis (DFA). Uncertainty ranges for source contributions of dust determined by the GLUE model showed that the dry lake Hamoun Puzak is the dominant source for all dust samples from Zabol and cultivated land is a secondary source. We found marked spatial variance in the importance of regional dry lake beds as dust sources, and temporal persistence in dust emissions from Hamoun Puzak, despite very large areas of adjacent lake beds drying during the study period. Aeolian sediment fingerprinting studies can benefit considerably from the constraints provided by modelling frameworks, such as GLUE, for quantifying the uncertainty in dust provenance data.

KEY WORDS: Sediment fingerprinting, uncertainty, GLUE, atmospheric dust, Iran

1. Introduction

Constraining the source of atmospheric dust particles circulating in the ancient past as well as the present-day is essential to understand the manifold implications of dust in the Earth system (Ridgwell, 2002; Goudie and Middleton, 2006; Shao et al., 2011). Ancient dust deposits are also archives of long-term environmental change (Dietze et al., 2016); the best-known and longest being the >8 Myr loess record in China (Sun & Zhu 2010). Present-day dust storms trigger a series of negative off-site and on-site repercussions (Goossens, 2003). Off-site effects include respiratory disease in humans and animals, contamination of food and water supplies, and interference with traffic safety, machinery, and electronics. On-site effects include the loss of soil organic matter, nutrients, and overall agricultural productivity (Goudie and Middleton, 2006). From this perspective, identifying sources of dust and quantifying multi-source contributions and their uncertainties is a key step towards hazard mitigation, especially in drylands.

A diverse range of techniques have been employed for tracing sources of atmospheric dust, including isotopic ratios (e.g., Krom et al., 1999; Nakano et al., 2004; Grousset and Biscaye, 2005; Chen et al., 2007; Cao et al., 2008; Wang et al., 2005; Rio-Salas et al., 2012; Yang et al., 2009); mineralogical and chemical characteristics (Shen et al., 2009); meteorological data (Rezazadeh et al., 2013; Nabavi et al., 2016; Ge et al., 2016; Rashki et al., 2017); synthesis of isotopic and geochemical data (e.g., Aarons et al., 2017; Wei et al., 2017; Chavagnac et al., 2008); synthesis of trace element and water-soluble ion analyses (Dahmardeh Behrooz et al., 2017a,b); numerical simulation (Hamidi et al., 2014; Nabavi et al., 2017); satellite data (Long et al., 2016; Cherboudj et al., 2016; Schepanski et al., 2012); and multidisciplinary approaches (Yan et al., 2015; Cao et al., 2015). While most of the studies listed above are highly successful at inferring dust sources, we note that in many cases the uncertainties associated with ascribing provenance are not considered formally. This is an important omission for two reasons: 1) airborne dust is commonly generated simultaneously from multiple populations and areas of fine-grained particles; and 2) these multiple populations are, in turn, typically an amalgam generated from different sources and mixed to differing degrees over timescales ranging from geological to individual storm events. In other words, dust provenance presents a very challenging mixing problem and hence uncertainty is fundamental. These two points ultimately stem from geomorphic processes of fine-particle production, transport, deposition, and reworking.

Sediment fingerprinting is widely used to quantify source contributions of fluvial sediments (e.g., Collins et al., 1997; Walling, 2005; Stone et al., 2014; Zhou et al., 2016a; and Manjoro et al., 2017) and its application to aeolian studies is growing (e.g., Liu et al., 2016; and Gholami et al., 2017a,b). Moreover, the uncertainties involved with this method are gaining increased attention (Walling, 2013). In order to manage and quantify the uncertainty in fluvial sediment fingerprinting, some studies have applied a Monte Carlo simulation framework (e.g., Motha et al., 2003; Collins et al., 2012; Voli et al., 2013; Smith and Blake, 2014; Stone et al., 2014; Sherriff et al., 2015; and Vale et al., 2016). Similarly, Bayesian approaches are also applied to fingerprinting aeolian sands (Gholami et al., 2017b) and fluvial sediments (e.g., Massoudieh et al., 2013; Cooper et al., 2014; Cooper et al., 2015; Stewart et al., 2015; and Abban et al., 2016). Yet, several challenges remain in adequately capturing the uncertainty associated with diverse aeolian dust sources and pathways (Walling, 2013) and we suggest that techniques developed in other disciplines may offer a way forward (Gholami et al., 2017b).

First proposed for hydrological modelling by Beven and Binley (1992), GLUE (Generalized Likelihood Uncertainty Estimation) has gained much favour as a tool for evaluating uncertainty estimates (e.g., Hassan et al., 2008; Zhou et al., 2016b; Viola et al., 2009; Mantovan and Todini, 2006; Gong et al., 2011). Here, we apply GLUE to the problem of dust provenance in the Sistan-Hamoun region on the Iran-Afghanistan border. Since it constitutes a major dust source for south-west Asia, Sistan has been the focus of numerous previous investigations (e.g., Goudie and Middleton, 2006; Rashki et al., 2012, 2013 a,b, 2015; Alizadeh Choobari et al., 2014). Recent work has generated an important dataset of dust samples from a meteorological station at Zabol, which has been analyzed geochemically to provide qualitative estimates of source (Dahmardeh Behrooz et al., 2017a) and the temporal variability of dust emissions (Dahmardeh Behrooz et al., 2017b). Here we provide the first attempt to formally quantify aeolian dust provenance and associated uncertainties with this dataset using GLUE.

2. Study area

The Sistan-Hamoun study area (Fig. 1) straddles the border between Afghanistan and the Sistan and Baluchestan province of south-eastern Iran (30˚5′ to 31˚28′ N and 61˚15′ to 61˚50′ E) (Rashki et al., 2012, 2013a). The Hamoun Lakes complex comprises three main lakes: Hamoun Hirmand, Hamoun Saberi, and Hamoun Puzak, which are recharged primarily from Afghanistan by the Hirmand (Helmand) River with smaller contributions from streams to the north and west (Esmaeili and Omrani, 2007). Following exceptionally high runoff, the lakes form a single body of water ~5700 km^2 in area and ~13 Mm^3 in volume (Sharifikia, 2013), though such events have become rare in recent decades

while dust emissions have grown correspondingly in magnitude (Goudie and Middleton, 2006; Rashki et al., 2012).

[Approximate location of figure 1]

The climate in the Sistan region is arid to hyper-arid, and land-use is chiefly linked to agriculture and fishing. At Zabol meteorological station (Fig. 1), mean rainfall is 55 mm y^{-1} and mean evaporation is >4000 mm y^{-1} (Moghaddamnia et al., 2009). The prevailing wind is the notorious Levar or "Wind of 120 Days" from the north, which in the summer is accelerated into a Low-Level Jet (LLJ) by a persistent high-pressure system over the Hindu Kush and the channeling effect of the surrounding topography (Alizadeh-Choobari et al., 2014; Kaskaoutis et al., 2016, 2017). As a result, the city of Zabol and its ~135,000 inhabitants experience dust storms of catastrophic proportions, resulting in Zabol ranking as the world's most polluted city for particulate matter less than 2.5 µm (PM2.5) in size (World Health Organisation, 2016).

3. Methods

3.1 Field sampling

We set out to characterise the soil materials for four different potential sources of atmospheric dust emissions to the north of Zabol city (Fig. 1): 1) the dry lake-bed of Hamoun Puzak (Fig. 2a); 2) the dry lake-bed of Hamoun Saberi (Fig. 2b); 3) cultivated arable farmland generally without crop-cover in summer (Fig. 2c); and 4) bare rangeland surfaces with sparse to negligible natural vegetation cover (Fig. 2d). A total of 31 surficial soil samples (<5 cm depth in a 30 cm^2 area) were collected from the four potential sources (Table 1). We sieved the soil samples with a 400-mesh sieve, retaining particles with a nominal geometric diameter of < 38.5 µm, which is roughly equivalent to the aerodynamic diameter of dust (Cao et al., 2008). After sieving, we retained about 5 g of dust-sized material from each sample.

[Approximate location of Figure 2]

During an exceptionally dusty summer period in Zabol (23 June to 4 October 2014), 57 atmospheric dust samples were collected at one- to four-day intervals (Table 1) with sampling apparatus fitted to the rooftop of the Department of Environmental Protection (5 m above ground level, 31˚N, 61.3˚E) in an outer suburban area with no major industrial activities nor local fugitive dust sources. Our two dust samplers (Model Chrono, Zambelli, Milan) were equipped with cyclones operating at a flow rate of 16.7 L/min as per the EU norms (Dahmardeh Behrooz et al, 2017a; 2017b). Total suspended-particle

(TSP) samples were collected in Teflon filters (0.45 µm pore size and 47 mm diameter) and then desiccated for 24-hours at 25 °C. Dust mass concentrations were measured gravimetrically by weighing the Teflon filters before and after sampling using an analytical balance (Adam model) with ±0.1 mg precision. We refrigerated all dust samples at 4˚C until chemical analysis (Dahmardeh Behrooz et al., 2017 a).

3.2 Laboratory analysis of water-soluble ions and trace elements

We measured the concentrations of 8 water-soluble ions in our samples (viz., Na^+, NH^+_4, K^+, Ca^{2+}, Mg^{2+}, Cl^-, NO^-_3, NO^-_2). Three cations (Na^+, NH^+_4 and K^+) were measured with a Shim-pack IC-C1 (Shimadzu DGU-12A) using 5-mM HNO_3 solution as eluent. Three anions (Cl^-, NO^-_3 and NO^-_2) were measured with a Shim-pack ICA1 (Shimadzu DGU-12A), using 2.5–mM phthalic acid combined with 2.4-mM tris-(hydroxymethyl) aminomethane as eluent (Lin, 2002). Two cations (Ca^{2+} and Mg^{2+}) were measured via flame atomic absorption spectrometry (Philips, PU9400X, England).

After acid digestion, all samples were analyzed to determine the concentrations of 16 trace elements (viz., Al, As, Au, Co, Cr, Cu, Fe, Li, Mg, Mn, Ni, Pb, Pt, Sn, Sr, and Zn) via Inductively Coupled Plasma Atomic Emission Spectroscopy (ICP-OES, Perkine Elmer, Optima 2000, USA). Further details of sampling and laboratory procedures are given in Dahmardeh Behrooz et al. (2017a, b).

3.3 Two-stage method: Kruskal-Wallis test and discriminant function analysis

The measurements of 8 water-soluble ions and 16 trace elements form the basis of the sediment fingerprinting method aimed at identifying the source contribution of the Zabol dust samples. We adopt a two-stage statistical procedure following the approach of Collins et al. (1997) to identify the most suitable tracers for source discrimination. In stage one we tested the primary ability of tracers to discriminate dust sources using the Kruskal-Wallis H test. Tracers with critical values at the 95 % confidence levels or better were taken to the second stage in which we identified optimum composite fingerprints using a stepwise discriminant function analysis based on minimization of Wilk's lambda.

3.4 Generalised Likelihood Uncertainty Estimation (GLUE)

GLUE was first devised by Beven and Binley (1992) as a means of sensitivity analysis and uncertainty estimation in environmental model outputs. We use GLUE to quantify the uncertainty in the sediment fingerprinting results via the following five steps:

1) Random sampling of parameter sets (300,000 iterations) are conducted using the Latin Hypercube Sampling (LHS) method (Zhou et al, 2016b), by assuming source contributions from each source are non-negative and that total contributions sum to unity. Due to the lack of prior information, we used a uniform distribution as the prior distribution for all parameters.

2) Selection of a likelihood function and behavioral parameter thresholds. Here, we adopt the Nash–Sutcliffe coefficient (ENS) as the likelihood function (Jin et al, 2010):

$$ME = 1 - \frac{\sum(O_{obs} - O_{sim})}{\sum(O_{obs} - \dot{Q}_{obs})} = 1 - \frac{\sigma_i^2}{\sigma_{obs}^2} \quad \text{(eq.1)}$$

where $\dot{Q}_{obs}$ is the mean value of the observed tracer concentration; O_{sim} is the simulated tracer concentration; O_{obs} is the observed tracer concentration; σ^2_i is the error variance for the *i*th model (i.e., the combination of the model and the *i*th parameter set) and σ^2_{obs} is the variance of the observations.

3) Sampled parameter sets from step 1 are input to the mixing model (equation 2) and the likelihood function is calculated for each parameter set as:

$$C_{dust} = C_{Sources} \times P \quad \text{(eq. 2)}$$

where P is an m dimensional column vector of sources contribution (sampled parameter sets), C_{dust} is an n-dimensional column vector of element concentration in sediment sample, $C_{Sources}$ is an n×m-dimensional matrix representing mean tracer concentration in sources (each row represents mean tracer concentration in each source), where n is the number of optimum composite fingerprints (n=5) and m is the number of dust sources (m=4).

4) Parameter sets are divided into behavioural and non-behavioural types with respect to a threshold value (Zhou et al, 2016). In this step, those parameter sets that have likelihood functions greater than a threshold value were classified as behavioural parameter sets. For the next step, non-behavioural parameter sets were discarded.

5) For behavioural parameter sets, likelihood weights are rescaled such that they sum to one, then each parameter is sorted and we calculate cumulative distributions for each parameter. Quintiles and uncertainty intervals are calculated via the cumulative distributions.

3.5 Geospatial analysis and climate data

Landsat data were downloaded from the United States Geological Survey's Earth Explorer, and all analysis was conducted within ArcGIS 10.3. Quantitative analysis of water extent was conducted using a modified Normalized Difference Water Index (NDWI), based on the green (Band 3) and short-wave infrared (Band 6) bands of Landsat 8 data (Xu, 2006). Climate data are taken from the Hourly Global Surface Data (DS3505) dataset for the Zabol station (World Meteorological Organization ID: 40829), accessed via the legacy Climate Data Online (CDO) portal of the National Oceanic and Atmospheric Administration's (NOAA) National Climatic Data Centre (NCDC) online (available at https://www7.ncdc.noaa.gov/CDO/dataproduct). To calculate back-trajectories for the air mass affecting Zabol during selected peak dust events of the observation period, we use NOAA's Hysplit model (summarized in Stein et al., 2015). Ensemble runs for the 24 hours preceding peak dust events were run based on airflow at 50, 100 and 500 m above the land surface. Additional remote sensing data regarding atmospheric dust flux and dust deposition was derived from NASA's Earthview platform in the form of a) visible MODIS imagery from July 2014, b) the MERRA-2 monthly PM2.5 dust deposition product for July 2014 (see Gelaro et al., 2017) and c) the AURA Ozone Monitoring Instrument (OMI) Aerosol Index product for July 2nd (Torres, 2006), near the start of the observed period of study.

4. Results

4.1 Kruskal-Wallis test and discriminant function analysis

The results of the Kruskal-Wallis tests (Table 2) indicate that among the twenty-four measured properties (8 water-soluble ions and 16 element concentrations), thirteen trace elements (Mg, Sr, Li, Fe, Cr, Cu, As, Ni, Pb, Mn, Co, and Sn) and one ion (Ca^{2+}) show statistically significant differences at the 95 %-level between the four potential dust sources (the two dry lake beds, cultivated farmland, and rangeland areas of natural vegetation cover). Trace elements clearly out-performed water-soluble ions for tracking spatial sources of dust. Thirteen trace elements were passed to stage-two for stepwise discriminant function analysis (DFA). The DFA yielded five trace elements (Fe, Sr, Mn, Cr and Pb) with optimum composite fingerprints that correctly discriminate 87 % of our source samples (Table 2 and Fig. 3).

[Approximate location of Figure 3]

4.2 Using GLUE to constrain uncertainty in the source contributions of dust

Uncertainty intervals of source contributions estimated by the GLUE-mixing model at the 95 % confidence level are presented in Figure 4. These results show that the most important dust source is clearly Hamoun Puzak (Figs. 4a and 5). Median contributions from this lake-bed span 29 to 88 % (samples 33 and 45, respectively). Hamoun Saberi is a less important source for our samples. Median contributions from this lake bed span 3 to 24 % (samples 11 and 33, respectively) (Fig. 4b). The sparsely vegetated rangeland is the least active dust source. Median contributions span 2 to 22 % (samples 45 and 34, respectively) (Fig. 4c). Cultivated farmland is recognized as the second-most important source for all of 57 samples. Median contributions from farmland span 4 to 25 % (samples 23 and 34, respectively) (Figs. 4d). For most samples, the lower-limit of predicted uncertainty is zero for contributions from the three sources other than Hamoun Puzak (Figs. 4b-d). Figure 5 presents an overview of the source contributions with all samples plotted together as a frequency histogram.

Overall, a strong correlation (Pearson's r = 0.783, p <0.001) can, unsurprisingly, be seen between dust flux and the logarithm of the windspeed, with a threshold of around 10 m s^{-1}. However, no significant correlation is observed between the relative contribution of Hamoun Puzak and Saberi, and either the windspeed (Pearson's r = -0.06, p = 0.66) or wind direction (Pearson's r = 0.238, p = 0.07).

[Approximate location of Figure 4]

[Approximate location of Figure 5]

5. Discussion

Sediment fingerprinting is a highly effective technique for quantifying source contributions of fluvial sediments (e.g. Collins et al., 1997; Walling, 2005; Stone et al., 2014; Zhou et al., 2016a; Manjoro et al., 2017) and aeolian sands (e.g. Liu et al., 2016; Gholami et al., 2017a,b). Here we build upon this approach by exploring the potential of the GLUE methodology for distinguishing spatially proximal aeolian dust sources with similar underlying geology and geomorphology. We demonstrate its efficacy at formally quantifying the uncertainty distributions associated with aeolian dust fingerprinting due to spatial and temporal variation in the dust cycle. Further, we use the method to reveal spatial complexity—alongside an unexpected lack of temporal complexity—in the nature of the dust sources.

5.1 Environmental context of dust emissions

The strong correlation between dusty days and the surface area of exposed lake floors indicates that i) dust storms in the Sistan-Hamoun region are directly related to the dryness of the Hamoun Lakes, and ii) these lake beds are the main source of dust emissions (Goudie and Middleton 2006; Rashki et

al., 2012; 2013a; 2013b; 2015). Such relationships are not uncommon, as worldwide observations suggest that exposed dry lake beds can govern the frequency and intensity of dust storms; for example, at Owens Lake, USA (Reheis et al., 2009); Aral Sea, Uzbekistan (Breckle et al., 2012); Makgadikgadi pan complex and Etosha Pan, southern Africa (Prospero et al., 2002; Mahowald et al., 2003; and Washington et al., 2003); and Kata Thandi-Lake Eyre, Australia (Baddock et al., 2009).

The frequency and magnitude of dust emissions from the Hamoun Lakes has also been related to annual/decadal scale variations in the surface area of the lakes, which varies dramatically. At its maximum extent, observed following the 1998 spring-melt Hirmand River floods (Rashki et al., 2012a), the Hamoun lake complex forms a single body of water ~4500 km^2 in area. This is comprised of Hamoun Hirmand (~1400 km^2), Hamoun Saberi (~1400 km^2) and Hamoun Puzak (~1700km^2), with Hamoun Baringak forming a series of smaller lakes and spillways between Saberi and Puzak. During more typical lake-full episodes, these bodies of water are not conjoined; for instance, during the spring of 1996 (Figure 6a), Hamoun Saberi spanned ~815 km^2 and Hamoun Puzak spanned 375 km^2 (Hamoun Baringak is here considered part of the western extent of the Puzak basin). Hamoun Hirmand lies mostly downwind of Zabol, and hence is not considered further. Between 1999 and 2010, a prolonged drought likely related to the El Nino Southern Oscillation resulted in the rapid and sustained desiccation of the Hamoun Lakes, with a concomitant increase in the frequency of dusty days (Rashki et al., 2012; 2013b). Since 2010, lake levels have been highly variable (Fig. 6), with a return to lake-full conditions experienced around 2011, and a subsequent return to large areas of exposed dry lake beds in more recent years.

Such changes can also develop rapidly. Within the timeframe of this study (June-October 2014), Hamoun Puzak and Hamoun Saberi lost around 295 km^2 and 640 km^2 of water surface area, respectively (i.e. 98.5% and 99.9% of their extent on June 14th) (Fig. 7). The small, shallow Hamoun Baringak lakes, directly to the north of Zabol, dried especially early in the season, with almost all water lost by July 2014. This desiccation affected Hamoun Saberi and Puzak proportionally at very similar rates, but Saberi's larger surface area at the start of this study led to greater absolute change in the lake floor exposure area. During this period, there was no rainfall recorded at the Zabol meteorological station, but the persistent 'Wind of 120 Days' blew from 327° ± 36° during June-October, with daily average windspeeds up to 15 m s^{-1} (~35 mph) and 50 of the 138 days of the study period exceeding daily averages of ~9 m s^{-1} (~20 mph).

[Approximate location of Figure 6]

[Approximate location of Figure 7]

5.2. Dust sources: dry beds of Hamoun Lakes

The GLUE results (Figs 4 and 5) reveal that the dominant source of dust collected at Zabol is Hamoun Puzak, and also that in general, the dust sources vary little over the three-month period from June to the beginning of October, 2014. This finding is unexpected, for a number of reasons. Firstly, as the wind at Zabol during this period comes from the northwest to north-northwest (327° ± 36°), the most obvious candidate source of Zabol dust is the upwind Hamoun Saberi (Figures. 1 and 7). Yet, consistently, Hamoun Puzak contributes ~40-90% (uncertainties included) of the dust received at Zabol. Furthermore, given the rapid increase in Saberi's exposed dry bed during the early period of sampling, its contribution would be expected to increase proportionally over this period. But Saberi's contributions actually vary little during the season (Fig. 4). When the surface area of the lakes is considered, either relative to lake-full conditions (Figure 8a and 8c), or as absolute surface areas (Figure 8b and 8d), there is little temporal relationship with the relative dust contributions of the two lake beds.

[Approximate location of Figure 8]

Similarly, investigation of the meteorological conditions during June-October do not readily explain the dominance of Hamoun Puzak. There is no clear correlation with either wind magnitude, or direction, that can readily explain the dominance of Puzak, and no obvious explanation for the occasional excursions when other sources contribute markedly more. For instance, on August 27th replicate samples were collected (S33 and S34 in Fig. 4) and yield consistent results (note that, for consistency, only one of these samples is included in Figs. 8 and 9). Satellite aerosol observations, modelled dust deposition, and aerosols indices (Figure 10), whilst confirming the regional importance of the Hamoun Lakes, do not readily identify localized sources due to their relative spatial coarseness.

These results suggest that Hamoun Puzak—or at least Hamoun Baringak at the western margin of Hamoun Puzak, where the source samples were collected (Fig. 1)—is a prolific and persistent source of dust over Zabol irrespective of the existence of large adjacent alternative sources. Why is Hamoun Puzak such an effective dust emitter? And why, despite its size and position directly upwind of Zabol, does Hamoun Saberi contribute relatively little? We propose that several factors have an influence, as follows.

[Approximate location of Figure 9]

[Approximate location of Figure 10]

First, let us consider the hydrological setting and sedimentology of the area. The Hamoun Lakes are predominantly fed with water from the Hirmand River to the east, with the Khash River also feeding directly into Hamoun Puzak from the east. Hamoun Saberi is fed largely from the north by the Harut and Farah rivers. The sampled region around Hamoun Baringak and Hamoun Puzak lies in series of channels and small closed basins which act as spillways connecting the lakes during lake-full episodes. Such areas are likely to have distinctly different sedimentology from lake bed areas subject to direct lacustrine sedimentation (King et al., 2011, Sweeney et al., 2011). Evidence that these sediments are distinct from those of Hamoun Saberi is implicitly provided in the primary function of the DFA used here to define the characteristics of these dusts (Fig. 3). The wind regime necessary for aeolian transport to Zabol from Hamoun Baringak is compatible with this zone being a dominant source, as northerly orientation lies well within the 327° ± 36° (one sigma) direction of the observed winds. It may also be that the transport pathways associated with the low-level jet from the north are strongly impacted by topography. We note that wind streaks evident on the satellite imagery of the region (visible in the northern and western part of Figure 7) suggest that topography is steering and deflecting local winds in a complex manner. For instance, topographic roughness caused by rocky hills around Hamoun Saberi may reduce effective winds at the surface. Further detailed analysis of the possible role of topographic steering of the winds in this, and other comparable studies, is clearly desirable, but does require high-resolution data and sophisticated modeling of the wind field to achieve substantial results.

The mean orientation of the seasonal winds, however, raises another question: Why does Hamoun Saberi, which lies directly upwind of Zabol, not contribute more to Zabol's dust flux, especially during the latter part of our study when an additional 640 km^2 of dry lake bed became exposed? It is well-reported that dust production can be spatially highly variable, even at sub-basin scales (Mahowald et al., 2003, Reheis et al., 2002, Bullard et al., 2008). One possibility relates to the differing geochemistry of the sediments that can promote the formation of protective crusts. Field experiments have shown that dry river courses when replenished frequently with fine-grained fluvial sediment can be much more effective at producing deflatable dust relative to playas and, counter-intuitively, playa centres are relatively low emission sources (Sweeney et al., 2011, King et al., 2011). Dry lake-bed deposits from the Mojave in the western US, for instance, have been reported to yield less dust than those with fluctuating water-levels (Reynolds et al., 2007), and the progressive and rapid desiccation of Hamoun

Saberi during the study period may have been simply unfavourable for the generation of deflatable dust.

Conversely, it may be that exogenic water supply from the northerly channels sufficiently dampened the surface to limit additional deflation. We note that shallow flooding was observed during the field sample collection, despite the lack of rain observed either in Zabol, or the fortnightly Landsat images. Over longer timescales, rates of aeolian erosion have been shown to inversely relate to soil moisture (Whitney et al., 2015). Although the whole region is sparsely vegetated, the role of vegetation in influencing surface roughness and thus susceptibility to aeolian erosion also cannot be overlooked (e.g. Cowie et al., 2013, Li et al., 2007). Lastly, we point to the cause of the additional 13% of variability, which was not well explained by the discriminant function analysis of the source sediments. This variability may imply that a significant component of Zabol dust derives from outside the immediate area of the Hamoun Lakes. Dust plumes transported from the Karakum desert in Turkmenistan are also known to affect much of southwest Asia, including the Sistan region (Kskaoutis et al., 2015), and may be a source of exogenous dust not accounted for among the four potential sources we sampled. To address these questions, we use the Hysplit model to calculate back-trajectories for three intervals characterized by high dust deposition during the study period (Figure 11). These confirm variability in both localized and regional wind trajectories for the high dust-flux days during period July to September 2014. The role of the Karakum in contributing long-distance flux is supported, over the 24-hour transport window modelled here (Figure 11a). However, there is also evidence of local and regional variability, with July and August winds coming locally via a north-northwesterly track (over a still largely inundated Hamoun Saberi), and the September peak in dust emission driven near Zabol by a due northerly wind, tracking directly over a desiccated Hamoun Baringak and Puzak (Figure 11b). This is likely related to seasonal variation of the Caspian Sea – Hindu Kush Index (CasHKI), a broadly east-west atmospheric pressure dipole between 40–50°N, 50–55°E and 35–40°N, 70–75°E (Kaskaoutis et al., 2016, 2017). This suggests that the interplay of atmospheric and hydrological controls on dust emission is crucial in this region.

[Approximate location of Figure 11]

5.3. Dust sources: cultivated and uncultivated rangeland areas

The connections between land management, agriculture and aeolian dust emissions are well documented (Wiggs and Holmes, 2011, Okin et al., 2001), and the role of agriculture in exacerbating drought-driven dust events such as the decade-scale ‘Dust Bowl’ of 1930s USA is clearly established

(Worster, 2004). We find that the cultivated cropland to the north of Zabol is the region's second-largest overall source of dust (Fig. 4), slightly out-stripping Hamoun Saberi, and contributing substantially more than uncultivated rangeland with sparse vegetation. Desertification, by which we mean mainly arid land degradation, has been recognized in other regions of Iran (Sepehr et al., 2007), and given the difficulties for agriculture in such an extremely dry and hot climate, it becomes apparent that sustainable land management is difficult to achieve. The spread of wind erosion is challenging land managers worldwide - from the Argentinian Pampas (Buschiazzo and Zobeck, 2008) to the Tibetan Plateau (Zhang et al., 2012) and even temperate regions such as southern Sweden (Barring et al., 2003). The findings here that cultivation-based farming is the second largest contributor to Zabol's dust flux (with median contributions of 4-25% for individual samples) highlights an anthropogenic dust source that could be quelled with alternative farming practices.

6. Conclusion

Identifying source(s) of aeolian sediments (sand and dust) is essential to improve planning and management of arid and semi-arid regions. Here we present a quantitative sediment fingerprinting approach coupled with the GLUE methodology to quantify source contributions of dust to the city of Zabol in the Sistan-Hamoun region of south-east Iran. Zabol consistently ranks globally as one of the most susceptible to fine (PM2.5 and PM10) aerosol pollutants. Using GLUE, we have assigned quantitative estimates of the relative contributions of four potential dust sources: two dry lake beds (Hamoun Puzak and Hamoun Saberi), cultivated land, and sparsely-vegetated uncultivated rangeland. The dry bed of Hamoun Puzak is the major source supplying sediment for dust samples, with cultivated land contributing more than Hamoun Saberi or rangeland areas. Robust estimates of uncertainty reveal that whilst the other three dust sources are broadly similar in magnitude, the western end of Hamoun Puzak (Hamoun Baringak) is undoubtedly the main source.

The samples used for these analyses were collected over a three-month period, during the first half of which the surface water extent of both Puzak and Saberi lakes decreased by > 98%. Yet, the relative contributions from the different land classes remained remarkably consistent. We also note that despite a persistent seasonal wind bearing NW-NNW upon Zabol, the main dust source lies to the northerly segment of the winds observed. This suggests that either the median wind direction is not the most dust-bearing, or the transport pathways are more complex than suspected. Hysplit analyses suggest important temporal variations during the windy season.

Our results demonstrate both the potential and the necessity of combining quantitative provenancing techniques with robust uncertainty methods and, ultimately, improved land management. The straightforward approach of linking the main wind direction to a large and rapidly-drying lake bed (Hamoun Saberi) does not yield a good predictive outcome, in this case. Spatial variation in dust sources has been identified elsewhere, most strikingly at the Bodélé Depression in the Chadian Sahara (Washington et al., 2003); here we demonstrate the application of methods with the scope to identify such spatial variation from the point of receipt of the dust. We are unable to outline the exact reasons for Hamoun Puzak's susceptibility to aeolian erosion. However, we attribute notable influence to the geomorphological conditions of the western arm of the Puzak, with its array of interconnected small basins (Hamoun Baringak) and spillways proving more prone to generating dust emissions.

REFERENCES

Aaron, S. M., Blakowski, M. A., Aciego, S. M., Stevenson, E. I., Sims, K. W. W., Scott, S, R., and Aarons, C. (2017). Geochemical characterization of critical dust source regions in the American West. Geochimica et Cosmochimica Acta 215; 141-161. http://dx.doi.org/10.1016/j.gca.2017.07.024

Abban, B., Papanicolaou, A, N., Cowles, M. K., Wilson, C. G., Abaci, O., Wacha, K., Schilling, and K., Schnobelen, D. (2016). An enhanced Bayesian fingerprinting framework for studying sediment source dynamics in intensively managed landscapes. Water Resource Research, 52, 4646-4673. doi:10.1002/2015WR018030.

Alizadeh Choobari, O., Zawar-Reza, P., and Sturman, A. (2014). The "wind of 120 days" and dust storm activity over the Sistan Basin. Atmospheric Research, 143; 328-341. http://dx.doi.org/10.1016/j.atmosres.2014.02.001

Baddock, M. C., Bullard, J. E., and Bryant, R. G (2009). Dust source identification using MODIS: a comparison of techniques applied to the Lake Eyre Basin, Australia. Remote Sens Environ, 113:1511–28.

Barring, L., Jonsson, P., Mattsson, J. O. & Ahman, R. 2003. Wind erosion on arable land in Scania, Sweden and the relation to the wind climate - a review. *Catena*, 52**,** 173-190.

Beven, K. and Binley, A. (1992). The future of distributed models: Model calibration and uncertainty prediction. Hydrological Processes, 6(3), 279-298. doi: 10.1002/hyp.3360060305.

Breckle, S.W., Wucherer, W., Liliya, A., Dimeyeva, L. A., Nathalia, P., and Ogar, N.P. (2012). Aralkum - a man-made desert: the desiccated floor of the Aral Sea (Central Asia). Springer; 2012486.

Bullard, J., Baddock, M., Mctainsh, G. & Leys, J. 2008. Sub-basin scale dust source geomorphology detected using MODIS. *Geophysical Research Letters*, 35.

Buschiazzo, D. E. & Zobeck, T. M. 2008. Validation of WEQ, RWEQ and WEPS wind erosion for different arable land management systems in the Argentinean Pampas. *Earth Surface Processes and Landforms*, 33**,** 1839-1850.

Cao, H., Amiraslani, F., Liu, J., and Zhou, N. (2015). Identification of dust storm source areas in West Asia using multiple environmental datasets. Science of the Total Environment, 502; 224-235. http://dx.doi.org/10.1016/j.scitotenv.2014.09.025

Cao, J. J., Zhu, C. S., Chow, J. C., Liu, W. G., Han, Y. M., and Watson, J. G. (2008). Stable carbon and oxygen isotopic composition of carbonate in fugitive dust in the Chinese Loess Plateau. Atmospheric Environment, 42; 9118-9122. doi:10.1016/j.atmosenv.2008.09.043

Chavagnac, V., Lair, M., Milton, J. A., Lioyd, A., Croudace, I .W., Palmer, M. R., Green, D. R. H., and Cherkashev, G. A. (2008). Tracing dust input to the Mid-Atlantic Ridge between 14°45′N and 36°14′N: Geochemical and Sr isotope study. Marine Geology, 247; 208-225. doi:10.1016/j.margeo.2007.09.003

Chen, J., Li, G., Yang, J., Rao, W., Lu, H., Balsam, W., Sun, Y., and Ji, J. Nd and Sr isotopic characteristics of Chinese deserts: Implications for the provenances of Asian dust. Geochimica et Cosmochimica Acta, 71; 3904-3914.

Cherboudj, I., Beegum, S. N., and Ghedira, H. (2016). Identifying natural dust source regions over the Middle-East and North-Africa: Estimation of dust emission potential. Earth Science Review. http://dx.doi.org/10.1016/j.earscirev.2016.12.010

Collins, A. L., and Walling, D. E. (2007). Sources of fine sediment recovered from the channel bed of lowland groundwater-fed catchments in the UK. Geomorphology, 88, 120–138. doi:10.1016/j.geomorph.2006.10.018

Collins, A.L., Walling, D.E., and Leeks, G.J.L. (1997). Fingerprinting the origin of fluvial suspended sediment in larger river basins: combining assessment of spatial provenance and source type. Geografiska Annaler, 79, 239–254.

Collins, A.L., Zhang, Y., Walling, D.E., Grenfell, S.E., Smith, P., Grischeff, J., … Brogden, D. (2012). Quantifying fine-grained sediment sources in the River Axe Catchment, southwest England: Application of a Monte-Carlo numerical modelling framework incorporating local and genetic algorithm optimisation. Hydrological Processes, 26 (13), 1962–1983. doi:10.1002/hyp.8283.

Cooper, R. J., Krueger, T., Hiscock, K. M., & Rawlins, B. G. (2014). Sensitivity of fluvial sediment source apportionment to mixing model assumptions : A Bayesian model comparison. Water Resources Research, 9031–9047. doi:10.1002/2014WR016194.

Cooper, R. J., Krueger, T., Hiscock, K. M., & Rawlins, B. G. (2015). High-temporal resolution fluvial

sediment source fingerprinting with uncertainty: A Bayesian approach. Earth Surface Processes and Landforms, 40(1), 78–92. doi:10.1002/esp.3621

Cowie, S. M., Knippertz, P. & Marsham, J. H. 2013. Are vegetation-related roughness changes the cause of the recent decrease in dust emission from the Sahel? *Geophysical Research Letters*, 40, 1868-1872.

Dahmardeh Behrooz, R., Esmaili-Sari, A., Bahramifar, N., and Kaskaoutis, D. G. (2017a). Analysis of the TSP, PM10 concentrations and water-soluble ionic species in airborne samples over Sistan, Iran during the summer dusty period. Atmospheric Pollution Research, 8; 403-417. http://dx.doi.org/10.1016/j.apr.2016.11.001

Dahmardeh Behrooz, R., Esmaili-Sari, A., Bahramifar, N., and Kaskaoutis, D. G., Saeb, K., and Rajaei, F. (2017b). Trace-element concentrations and water-soluble ions in size-segregated dust-borne and soil samples in Sistan, southeast Iran. Aeolian Research, 25; 87-105. http://dx.doi.org/10.1016/j.aeolia.2017.04.001

Del Rio-Salas, R., Ruiz, J., De la O-Villanueva, M., Valencia-Moreno, M., Moreno,-Rodriguez, V., Gomez-Alvarez, A., Grijalva, T., Mendivil, H., Paz-Moreno, F., and Meza-Figueroa, D. (2012). Tracing geogenic and anthropogenic sources in urban dusts: Insights from lead isotopes. Atmospheric Environment, 60; 202-210. http://dx.doi.org/10.1016/j.atmosenv.2012.06.061

Esmaeili, A. and Omrani, M. (2007). Efficiency analysis of fishery in Hamoon lake using DEA approach. J. Appl. Sci, 7; 2856-2860.

Ge, Y., Abuduwaili, J., Ma, L., Wu, N., and Liu, D. (2016). Potential transport pathways of dust emanating from the playa of Ebinur Lake, Xinjiang, in arid northwest China. Atmospheric Research, 178-179; 196-206. http://dx.doi.org/10.1016/j.atmosres.2016.04.002

Gelaro, R., McCarty, W., Suárez, M. J., Todling, R., Molod, A., Takacs, L., Randles, C. A., Darmenov, A., Bosilovich, M. G. & Reichle, R. (2017) 'The modern-era retrospective analysis for research and applications, version 2 (MERRA-2)'. Journal of Climate, 30 (14), pp. 5419-5454.

Gholami, H., Middleton, N., Nzari Samani, A., and Wasson, R. (2017a). Determining contribution of sand dune potential sources using radionuclides, trace and major elements in central Iran. Arab J Geosci, 10:163. doi. 10.1007/s12517-017-2917-0.

Gholami, H., Telfer, M. W., Blake, W. H., and Fathabadi, A. (2017) Aeolian sediment fingerprinting using a Bayesian mixing model. Earth Surf. Process. Landforms, 42: 2365–2376. doi: 10.1002/esp.4189.

Gong, Y., Shen, Zh, Hong, Q., Liu, R., and Liao, Q. (2011). Parameter uncertainty analysis in watershed total phosphorus modeling using the GLUE methodology. Agriculture, Ecosystems and Environment 142; 246-255. doi:10.1016/j.agee.2011.05.015

Goossens, D. (2003). On-site and off-site effects of wind erosion. In: Warren A (ed) Wind erosion on agricultural land in Europe. European Commission, Luxembourg, pp. 29–38

Goudie, A. S. and Middleton, N. J. (2006). Desert dust in the global system. Springer.

Grousset, F. E. and Biscaye, P. E. (2005). Tracing dust sources and transport patterns using Sr, Nd and Pb isotopes. Chemical Geology, 222; 149-167. doi:10.1016/j.chemgeo.2005.05.006

Hamidi, M., Kavianpour, M. R., and Shao, Y. (2014). Numerical simulation of dust events in the Middle East. Aeolian Research, 13; 59-70. http://dx.doi.org/10.1016/j.aeolia.2014.02.002

Hassan, A. E., Bekhit, H. M., and Chapman, J. B. (2008). Uncertainty assessment of a stochastic groundwater flow model using GLUE analysis. Journal of Hydrology, 362; 89-109. doi:10.1016/j.jhydrol.2008.08.017

Kaskaoutis, D.G., Rashki, A., Francois, P., Dumka, U.C., Houssos, E.E., and Legrand, M. (2015). Meteorological regimes modulating dust outbreaks in southwest Asia: the role of pressure anomaly and Inter-Tropical Convergence Zone on the 1–3 July 2014 case. Aeolian Research. 18, 83–97.

Kaskaoutis, D. G., Houssos, E. E., Rashki, A., Francois, P., Legrand, M., Goto, D., Bartzokas, A., Kambezidis, H. D. & Takemura, T. (2016) 'The Caspian Sea–Hindu Kush Index (CasHKI): a regulatory factor for dust activity over southwest Asia'. Global and Planetary Change, 137 pp. 10-23.

Kaskaoutis, D. G., Rashki, A., Houssos, E. E., Legrand, M., Francois, P., Bartzokas, A., Kambezidis, H. D., Dumka, U. C., Goto, D. & Takemura, T. (2017) 'Assessment of changes in atmospheric dynamics and dust activity over southwest Asia using the Caspian Sea–Hindu Kush Index'. International Journal of Climatology, 37 (S1), pp. 1013-1034.

Kaskaoutis, D.G., Rashki, A., Houssos, E. E., Goto, D., and Nastos, P. T. (2014). Extremely high aerosol loading over Arabian Sea during June 2008: the specific role of the atmospheric dynamics and Sistan dust storms. Atmospheric Environment. Doi: 10.1016/j.atmosenv.2014.05.012

King, J., Etyemezian, V., Sweeney, M., Buck, B. J. & Nikolich, G. 2011. Dust emission variability at the Salton Sea, California, USA. *Aeolian Research*, 3**,** 67-79.

Krom, M.D., Cliff, R. A., Eijsink, L. M., Herut, B., and Chester, R. (1999). The characterisation of Saharan dusts and Nile particulate matter in surface sediments from the Levantine basin using Sr isotopes. Marine Geology, 155; 319-330.

Li, J., Okin, G. S., Alvarez, L. & Epstein, H. 2007. Quantitative effects of vegetation cover on wind erosion and soil nutrient loss in a desert grassland of southern New Mexico, USA. *Biogeochemistry*, 85**,** 317-332.

Liu, B., Niu, Q., Qu, J., and Zu, R. (2016). Quantifying the provenance of aeolian sediments using

multiple composite fingerprints. Aeolian Research, 22, 117-122. dx.doi.org/10.1016/j.aeolia.2016.08.002

Long, X., Li., N., Tie, X., Cao, J., Zhao, Sh., Huang, R., Zhao, M., Li, G., and Feng, Tian. (2016). Urban dust in the Guanzhong Basin of China, part I: A regional distribution of dust sources retrieved using satellite data. Science of the Toatal Environment, 541; 1603-1613. http://dx.doi.org/10.1016/j.scitotenv.2015.10.063

Mahowald, N. M., Bryant, R. G., del Corral., J., and Steinberger, L. (2002). Ephemeral lakes and desert dust sources. Geophys Res Lett, 30:1074. http://dx.doi.org/10.1029/2002GL016041

Manjoro, M., Rowntree, K., Kakembo, V., Foster, I., and Collins, A. L. (2017). Use of sediment source fingerprinting to assess the role of subsurface erosion in the supply of fine sediment in a degraded catchment in the Eastern Cape, South Africa. Journal of Environmental Management, 194, 27-41. dx.doi.org/10.1016/j.jenvman.2016.07.019

Massoudieh, A., Gellis, A., Banks, W. S., & Wieczorek, M. E. (2013). Suspended sediment source apportionment in Chesapeake Bay watershed using Bayesian chemical mass balance receptor modeling. Hydrological Processes, 27(24), 3363–3374. doi:10.1002/hyp.9429

Middleton NJ. (1986). Dust storms in the Middle East. J Arid Environ,10:83–96

Moghaddamnia, A., Ghafari, M.B., Piri, J., Amin, S., and Han, D. (2009). Evaporation estimation using artificial neural networks and adaptive neuro-fuzzy inference system techniques. Adv. Water Resour. 32, 88–97

Montovan, P. and Todini, E. (2006). Hydrological forecasting uncertainty assessment: Incoherence of the GLUE methodology. Journal of Hydrology, 330; 368-381. doi:10.1016/j.jhydrol.2006.04.046

Motha, J.A., Wallbrink, P.J., Hairsine, P.B., and Grayson, R.B. (2003). Determining the sources of suspended sediment in a forested catchment in southeastern Australia. Water Resources, 39 (3), 1056. doi:10.1029/2001wr000794.

Nabavi, S. O., Haimberger, L., and Samimi, C. (2016). Climatology of dust distribution over West Asia from homogenized remote sensing data. Aeolian Research, 21; 93-107. http://dx.doi.org/10.1016/j.aeolia.2016.04.002

Nabavi, S. O., Haimberger, L., and Samimi, C. (2017). Sensitivity of WRF-chem predictions to dust source function specification in West Asia. Aeolian Research, 24; 115-131. http://dx.doi.org/10.1016/j.aeolia.2016.12.005

Nakano, T., Yokoo, Y., Nishikawa, M., and Koyanagi, H. (2004). Regional Sr–Ndisotopic ratios of soil minerals in northern China as Asian dust fingerprints. Atmospheric Environment, 38; 3061-3067. doi:10.1016/j.atmosenv.2004.02.016

Okin, G. S., Murray, B. & Schlesinger, W. H. 2001. Degradation of sandy arid shrubland environments: observations, process modelling, and management implications. *Journal of Arid Environments*, 47**,** 123-144.

Rashki, A., Arjmand, A., and Kaskaoutis, D. G. (2017). Assessment of dust activity and dust-plume pathways over Jazmurian Basin, southeast Iran. Aeolian Research, 24; 145-160. http://dx.doi.org/10.1016/j.aeolia.2017.01.002

Rashki, A., Eriksson, P. G., Rautenbach, C. J. D., Kaskaoutis, D. G., Grote, W., and Dykstra, J. (2013a). Assessment of chemical and mineralogical characteristics of airborne dust in the Sistan region, Iran. Chemosphere, 90; 227-236. http://dx.doi.org/10.1016/j.chemosphere.2012.06.059

Rashki, A., Kaskaoutis, D. G., Francois, P., Kosmopoulos, P. G., and Legrand, M. (2015). Dust-storm dynamics over Sistan region, Iran: Seasonality, transport characteristics and affected areas. Aeolian Research, 16; 35-48.

Rashki, A., Kaskaoutis, D. G., Goudie, A. S., and Kahn, R. A. (2013b). Dryness of ephemeral lakes and consequences for dust activity: The case of the Hamoun drainage basin, southeastern Iran. Science of the Total Environment, 463-464; 552-564. http://dx.doi.org/10.1016/j.scitotenv.2013.06.045

Rashki, A., Kaskaoutis, D. G., Rautenbach, C. J. D., Eriksson, P. G. (2012a). Changes of Permanent Lake Surfaces, and Their Consequences for Dust Aerosols and Air Quality: The Hamoun Lakes of the Sistan Area, Iran. In: Hayder Abdul-Razzak (Eds.), Atmospheric Aerosols - Regional Characteristics. DOI: 10.5772/48776

Rashki, A., Kaskaoutis, D. G., Rautenbach, C. J. D., Eriksson, P. G., Qiang, M., and Gipta, P. (2012b). Dust storms and their horizontal dust loading in the Sistan region, Iran. Aeolian Research, 5; 51-62. doi:10.1016/j.aeolia.2011.12.001

Reheis, M. C., Budahn, J. R. & Lamothe, P. J. 2002. Geochemical evidence for diversity of dust sources in the southwestern United States. *Geochimica Et Cosmochimica Acta*, 66**,** 1569-1587.

Reheis, M., Budahn, J. R., Lamothe, P. J., and Reynolds, R. L. (2009). Compositions of modern dust and surface sediments in the Desert Southwest United States. J Geophys Res, 114: F01028. http://dx.doi.org/10.1029/2008JF001009

Reynolds, R.L., Yount, J.C., Reheis, M., Goldstein, H, Chavez Jr, P., Fulton, R, Whitney, J., Fuller, C., Forester, R.M. (2007). Dust emission from wet and dry playas in the Mojave Desert, USA. Earth Surface Processes and Landforms, 3; 1811-1827. https://doi.org/10.1002/esp.1515

Rezazadeh, M., Irannejad, P., and Shao, Y. (2013). Climatology of the Middle East dust events. Aeolian Research, 10; 103-109. http://dx.doi.org/10.1016/j.aeolia.2013.04.001

Schepanski, K., Tegen, I., and Macke. A. (2012). Comparison of satellite based observations of Saharan dust source areas. Remote Sensing of Environment, 123; 90-97. doi:10.1016/j.rse.2012.03.019

Sepehr, A., Hassanli, A. M., Ekhtesasi, M. R. & Jamali, J. B. 2007. Quantitative assessment of desertification in south of Iran using MEDALUS method. *Environmental Monitoring and Assessment*, 134**,** 243.

Shen, Z., Caquineau, S., Cao, J., Zhang, X., Han, Y., Gaudichet, A., and Gomes, L. (2009). Mineralogical characteristics of soil dust from source regions in northern China. Particulogy, 7; 507-512. doi:10.1016/j.partic.2009.10.001

Sherriff, S. C., Franks, S. W., Rowan, J. S., Fenton, O., & Ó'hUallacháin, D. (2015). Uncertainty-based assessment of tracer selection, tracer non-conservativeness and multiple solutions in sediment fingerprinting using synthetic and field data. Journal of Soils and Sediments, 15(10), 2101–2116. doi:10.1007/s11368-015-1123-5

Smith, H.G., and Blake, W.H. (2014). Sediment fingerprinting in agricultural catchments: A critical re-examination of source discrimination and data corrections. Geomorphology, 204, 177–191. doi:10.1016/j.geomorph.2013.08.003.

Stein, A. F., Draxler, R. R., Rolph, G. D., Stunder, B. J. B., Cohen, M. D. & Ngan, F. (2015) 'NOAA's HYSPLIT atmospheric transport and dispersion modeling system'. Bulletin of the American Meteorological Society, 96 (12), pp. 2059-2077.

Stewart, H. A., Massoudieh, A., & Gellis, A. (2015). Sediment source apportionment in Laurel Hill Creek, PA, using Bayesian chemical mass balance and isotope fingerprinting. Hydrological Processes, 29(11), 2545–2560. doi:10.1002/hyp.10364

Stone, M., Collins, A.L., Silins, U., Emelko, M.B., and Zhang, Y.S. (2014). The use of composite fingerprints to quantify sediment sources in a wildfire impacted landscape, Alberta, Canada. Science of the Total Environment, 473-474, 642–650. doi:10.1016/j.scitotenv.2013.12.052.

Sweeney, M. R., Mcdonald, E. V. & Etyemezian, V. 2011. Quantifying dust emissions from desert landforms, eastern Mojave Desert, USA. *Geomorphology*, 135**,** 21-34.

Sweeney, M. R., Zlotnik, V. A., Joeckel, R. M. & Stout, J. E. 2016. Geomorphic and hydrologic controls of dust emissions during drought from Yellow Lake playa, West Texas, USA. *Journal of Arid Environments*, 133**,** 37-46.

Torres, O. O. (2006) 'OMI/Aura Near UV Aerosol Optical Depth and Single Scattering Albedo. 1-orbit L2 Swath 13x24 km V003'.[in Greenbelt, MD, USA: Goddard Earth Sciences Data and Information Services Center (GES DISC). (Accessed: 6/11/18)

United Nations Environment Programme (UNEP) (2006). History of environmental change in the Sistan basin based on satellite image analysis: 1976–2005; 200660.

Vale, S. S., Fuller, I. C., Procter, J. N., Basher, L. R., and Smith, I. E. (2016). Characterization and quantification of suspended sediment sources to the Manawatu River, New Zealand. Science of the Total Environment, 543, 171–186. doi:10.1016/j.scitotenv.2015.11.003

Viola, F., Noto, L. V., Cannarozzo, G., and Loggia, G. L. (2009). Daily streamflow prediction with uncertainty in ephemeral catchments using the GLUE methodology. Physics and Chemistry of the Earth 34; 701-706.

Voli, M.T., Wegmann, K.W., Bohnenstiehl, D.R., Leithold, E., Osburn, C.L., and Polyakov, V. (2013). Fingerprinting the sources of suspended sediment delivery to a large municipal drinking water reservoir: Falls Lake, Neuse River, North Carolina, USA. Journal of Soils and Sediments, 13 (10), 1692–1707. doi:10.1007/s11368-013-0758-3.

Walling, D.E. (2005). Tracing suspended sediment sources in catchments and river systems. Science of the Total Environment, 344 (1-3), 159–184. doi:10.1016/j.scitotenv.2005.02.011.

Walling, D.E. (2013). The evolution of sediment source fingerprinting investigations in fluvial systems. Journal of Soils and Sediments, 13 (10), 1658–1675. doi:10.1007/s11368-013-0767-2.

Wang, Y. Q., Zhang. X. Y., Arimoto, R., Cao, J. J., and Shen, Z. X. (2005). Characteristics of carbonate content and carbon and oxygen isotopic composition of northern China soil and dust aerosol and its application to tracing dust sources. Atmospheric Environment, 39; 2631-2642. doi:10.1016/j.atmosenv.2005.01.015

Washington, R., Todd, M., Middleton, N.J., and Goudie, A. S. (2003). Dust storm source areas determined by the Total Ozone Monitoring Spectrometer and surface observations. Ann Assoc Am Geogr, 93: 297–313.

Wei, T., Dong, Z., Kang, Sh., Qin, X., and Guo, Zh. (2017). Geochemical evidence for sources of surface dust deposited on the Laohugou glacier, Qilian Mountains. Applied Geochemistry; 79; 1-8. http://dx.doi.org/10.1016/j.apgeochem.2017.01.024

Whitney, J. W., Breit, G. N., Buckingham, S. E., Reynolds, R. L., Bogle, R. C., Luo, L., Goldstein, H. L. & Vogel, J. M. 2015. Aeolian responses to climate variability during the past century on Mesquite Lake Playa, Mojave Desert. *Geomorphology*, 230**,** 13-25.

Wiggs, G. & Holmes, P. 2011. Dynamic controls on wind erosion and dust generation on west-central Free State agricultural land, South Africa. *Earth Surface Processes and Landforms*, 36**,** 827-838.

World Health Organisation (2016). WHO Global Urban Ambient Air Pollution Database. URL: http://www.who.int/phe/health_topics/outdoorair/databases/cities/en/ (Accessed 23/06/2018).

Worster, D. 2004. *Dust bowl: the southern plains in the 1930s*, Oxford University Press.

Xu, H. (2006). Modification of normalised difference water index (NDWI) to enhance open water features in remotely sensed imagery. International Journal of Remote Sensing, 27; 3025–3033. doi: 10.1080/01431160600589179

Yan, Y., Sun, Y., Ma., L., and Long, X. (2015). A multidisciplinary approach to trace Asian dust storms from source to sink. Atmospheric Environment, 105; 43-52. http://dx.doi.org/10.1016/j.atmosenv.2015.01.039

Yang, J., Li, G., Rao, W., and Ji, J. (2009). Isotopic evidences for provenance of East Asian Dust. Atmospheric Environment, 43; 4481-4490. doi:10.1016/j.atmosenv.2009.06.035

Zhang, D., Zhou, Z. H., Zhang, B., Du, S. H. & Liu, G. C. 2012. The effects of agricultural management on selected soil properties of the arable soils in Tibet, China. *Catena*, 93**,** 1-8. Prospero, J. M., Ginoux, P., Torres, O., Nicholson, S. E., and Gill, T. E. (2002). Environmental characterization of global sources of atmospheric soil dust identified with the Nimbus 7 total ozone mapping spectrometer absorbing aerosol product. Rev Geophys, 40: 2–31

Zhou, H., Chang, W., and Zhang, L. (2016a). Sediment sources in a small agricultural catchment: A composite fingerprinting approach based on the selection of potential sources. Geomorphology, 266, 11-19. dx.doi.org/10.1016/j.geomorph.2016.05.007

Zhou, R., Li, Y., Lu, D., Liu, H., and Zhou, H. (2016b). An optimization based sampling approach for multiple metrics uncertainty analysis using generalized likelihood uncertainty estimation. Journal of Hydrology, 540; 274-286. http://dx.doi.org/10.1016/j.jhydrol.2016.06.030.

Figure Captions

Figure 1: Sampling sites in the Sistan region: the dry-bed of Hamoun Puzak (HP); the dry-bed of Hamoun Saberi (HS); uncultivated range Land (RL); and cultivated Land (CL). Inset shows the hourly averaged wind regime for the period June-October 2014 (data source: National Climatic Data Centre, Climate Data Online).

Figure 2. Typical examples of the land surfaces we sampled. a) Hamoun Puzak dry lake-bed, b) Hamoun Saberi dry lake-bed, c) close-up view of cultivated agricultural land surface during the summer months, and d) sparsely vegetated, uncultivated rangeland.

Figure 3. Scatterplot constructed from the first and second functions derived from a stepwise DFA for the source groups including the four land (i.e. Hamoun Puzak (HP), Hamoun Saberi (HS), cultivated land (CL) and uncultivated rangeland (RL)). Five optimum fingerprints (Fe, Sr, Mn, Cr and Pb) were used to construct the scatterplot and 87% of the source samples are discriminated correctly.

Figure 4. GLUE results for dust source contributions yielding 95% confidence limits (with percentiles 2.5, 25, 50, 75 and 97.5). A) Hamoun Puzak; B) Hamoun Saberi; C) uncultivated rangeland; and d) cultivated land.

Figure 5. Summary of all source contributions plotted as a probability density function.

Figure 6. Decadal scale changes in the Hamoun Lakes. Following lake-full conditions in the late 1990s (a), a sustained decade of drought resulted in the exposure of large areas of dry lake-beds (b and c) and therefore potential dust sources. Since then, levels have varied and often changed rapidly (d, e and f). All images are infrared/red/green composites based on Landsat 5 and 8 imagery, using Bands 4/3/2 and 5/4/3 respectively. Vegetation is shown as red tones.

Figure 7. Changes in the surface extent of the Hamoun Lakes between June and September, 2014. Note the rapid desiccation during June and July, and resultant exposure of new surfaces for potential deflation.

Figure 8. The relative contributions of a) and b) Hamoun Puzak and c) and d) Hamoun Saberi, plotted alongside a) and c) the surface area of the lakes (expressed as a percentage of the 1996 lake-full condtions) and b) and d) the absolute surface area of the lakes. There is no consistent trend in dust provenance, despite the changing area of the potential sources. Solid lines indicate the median estimate, dashed lines the first and third quartiles and dotted lines the 2.5% and 97.5% bounds.

Figure 9. The dominant dust contribution from Hamoun Puzak (top; key for lines as in Figure 8), shown alongside the magnitude of dust collected at Zabol (bars), and the mean daily wind speed (thin solid line) and variance in mean wind direction (bold dashed line).

Figure 10. The dust plume affecting Zabol from the north is evident in remotely-sensed data from July 2014. a) The MODIS Corrected Reflectance Imagery (Red:Green:Blue) 500 m colour composite clearly shows the plume as a brown streak emanating from near the Hamoun Lakes and tracking southeastwards. b) The MERRA-2 PM2.5 monthly dust deposition reanalysis data also highlight the plume to the southeast of the Hamoun Lakes, as does c) the AURA OMI UV-derived Aerosol Index for July 4th, 2014.

Figure 11. Hysplit back trajectories for three dust events during the observation period in summer 2014 (4th July – white triangles, 14th August – grey circles, 4th September – black squares). a) Regional tracks over the 24 hours preceding the observations demonstrate the long-distance transport of dust, with a likely source in the Karakum Desert of Turkmenistan. b) Local dust transport pathways over the

Hamoun Lakes to Zabol demonstrate different pathways during the summer dust season, with early summer pathways (white triangles and grey circles) routing over the still-inundated Hamoun Saberi, and the September trajectory (black squares) coming over the desiccated Hamoun Baringak and Puzak.

Table 1: Summary characteristics of dust samples collected in Zabol during 21 June to 4 October, 2014.

dust sample no	Sampling date	W V* (m/s)	dust mass (ug/m^3)	dust sample no	Sampling date	W V* (m/s)	dust mass (ug/m^3)
1	23 June 2014	7.1	270.2	30	24 August 2014	6.5	300.15
2	25 June 2014	8.6	1180.5	31	25 August 2014	9	695.65
3	26 June 2014	6.3	380	32	26 August 2014	10.4	1100.15
4	29 June 2014	8.1	500.6	33	27 August 2014**	9.8	1052
5	30 June 2014	9	458	34	27 August 2014***	9.8	922.39
6	4 July 2014	9.5	7800	35	28 August 2014	8	606.29
7	5 July 2014	8.9	570.2	36	29 August 2014	7.4	271.3
8	11 July 2014	10.3	724	37	3 Sep 2014	10	3594.92
9	12 July 2014	10.5	1700.7	38	4 Sep 2014	11.4	3594.92
10	13 July 2014	10.5	831	39	5 Sep 2014	8.1	339.56
11	14 July 2014	8.9	370.3	40	6 Sep 2014	8.5	1243.88
12	18 July 2014	11.3	740.2	41	8 Sep 2014	6.1	186.21
13	19 July 2014	8.3	1800	42	10 Sep 2014	9.1	3188.85
14	21 July 2014	4.8	320.8	43	13 Sep 2014	7.4	296.8
15	3 August 2014	12.3	715.3	44	16 Sep 2014	4.6	213.77
16	4 August 2014	10	1600	45	17 Sep 2014	4.3	192.4
17	5 August 2014	5.1	216	46	19 Sep 2014	10.1	10785.5
18	6 August 2014	6.6	246.4	47	20 Sep 2014	8.5	1013.43
19	7 August 2014	10	1500	48	21 Sep 2014	4.9	111.76
20	8 August 2014	10	1803	49	22 Sep 2014	2.8	179.61
21	9 August 2014	10	480.04	50	24 Sep 2014	3.4	155.98
22	10 August 2014	8	560.04	51	26 Sep 2014	2.3	165.52
23	11 August 2014	9.1	4500	52	27 Sep 2014	5.5	274.83
24	12 August 2014	8.3	720	53	29 Sep 2014	4	90.31
25	13 August 2014	8.3	1480	54	30 Sep 2014	7.1	814.46
26	14 August 2014	11.5	9004.58	55	1 Oct 2014	5.1	413.15
27	16 August 2014	10.9	3529.4	56	2 Oct 2014	5.3	331.67
28	18 August 2014	5.1	126.74	57	3 Oct 2014	7.5	597.6
29	21 August 2014	8.3	498.5				

* W V indicates Wind Velocity; ** Sample collected on the day; *** Sample collected on the night.

Table 2: Results of a two-stage statistical process for selecting optimum composite fingerprints for distinguishing sources of dust.

Kruskal-Wallis H test			Stepwise DFA		
Fingerprint property	Chi-Square	P-value	Step	Entered fingerprint	Wilk's lambda
Trace elements			1	Fe	0.356
Au	6.79	0.079	2	Sr	0.188
Pt	1.58	0.664	3	Mn	0.081
Mg	20.83	0.000**	4	Cr	0.053
Al	1.48	0.686	5	Pb	0.033
Sr	20.6	0.000**			
Li	22	0.000**	*Statistically significant at P<0.05		
Fe	20.9	0.000**	** Statistically significant at P<0.01		
Cr	19.5	0.000**			
Cu	19.5	0.000**			
Zn	5.16	0.16			
As	9.9	0.019*			
Ni	20.75	0.000**			
Pb	9.58	0.022*			
Mn	20.24	0.000**			
Co	18.73	0.000**			
Sn	12.9	0.005**			
Ions					
Na^+	7.24	0.065			
NH^+_4	2.6	0.456			
K^+	4	0.254			
Cl^-	0.4	0.941			
NO^-_2	3.3	0.358			
NO^-_3	7.01	0.072			
Mg^{2+}	1.38	0.709			
Ca^{2+}	14.5	0.002**			

795

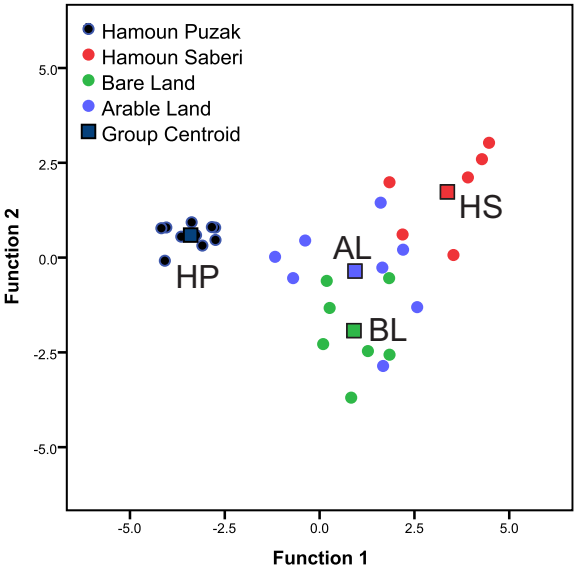
Hamoun Puzak
Hamoun Saberi
Bare Land
Arable Land
Group Centroid
HP
HS
AL
BL
Function 1
Function 2
5.0
2.5
0.0
-2.5
-5.0

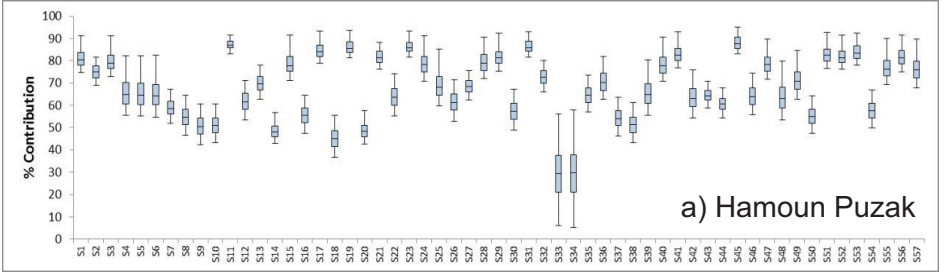
% Contribution
a) Hamoun Puzak

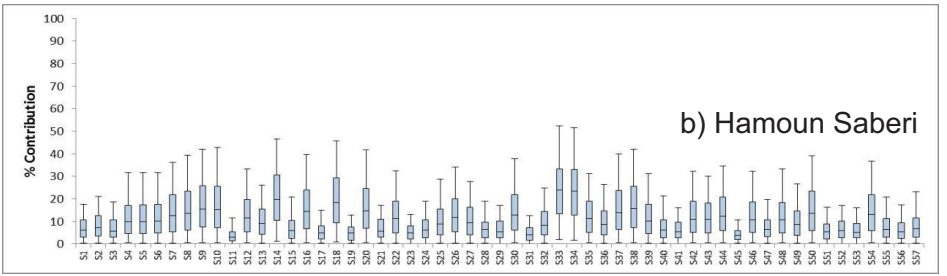
% Contribution
b) Hamoun Saberi

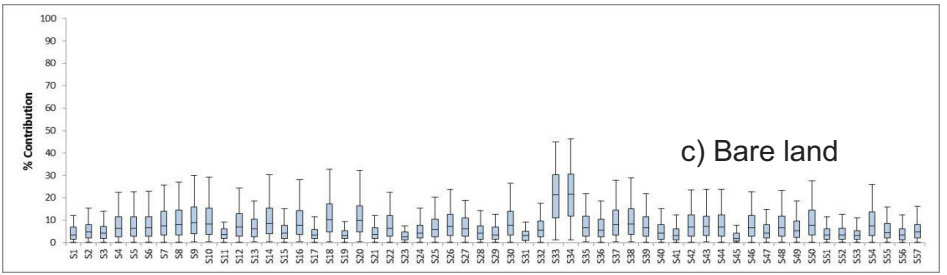
% Contribution
c) Bare land

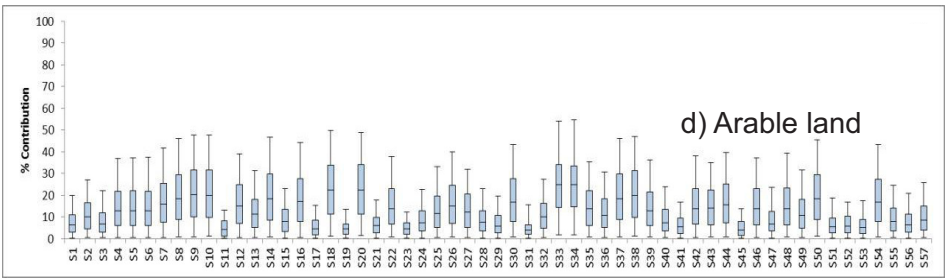
% Contribution
d) Arable land

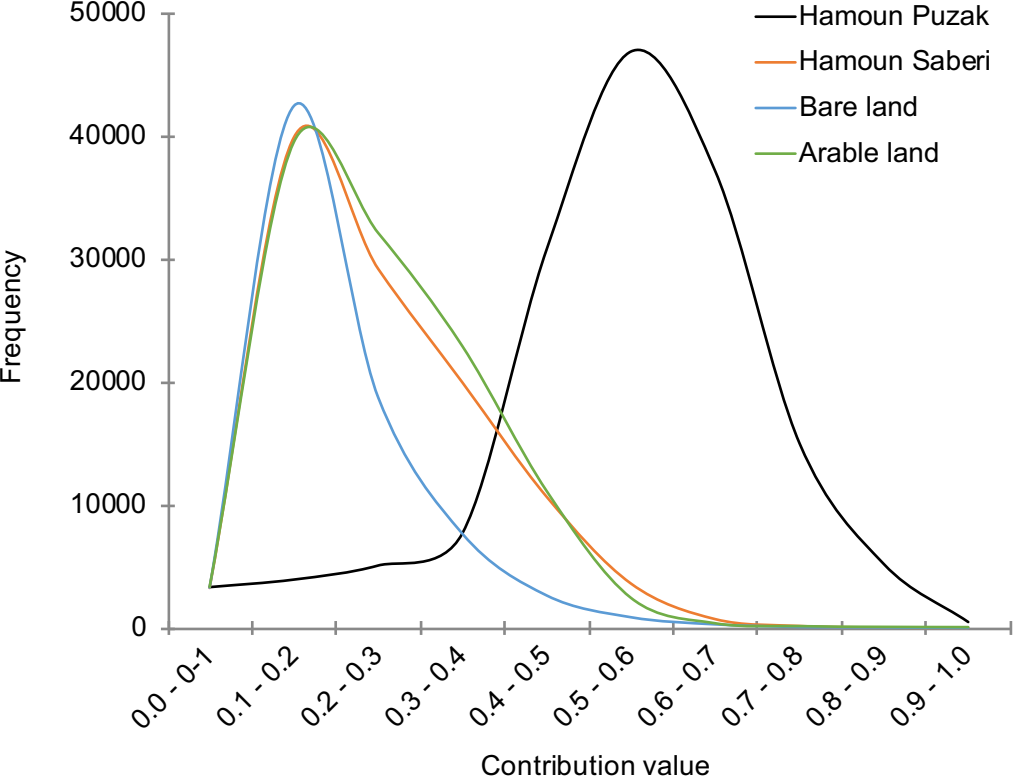
Hamoun Puzak
Hamoun Saberi
Bare land
Arable land
Frequency
50000
40000
30000
20000
10000
0
0.0 - 0.1
0.1 - 0.2
0.2 - 0.3
0.3 - 0.4
0.4 - 0.5
0.5 - 0.6
0.6 - 0.7
0.7 - 0.8
0.8 - 0.9
0.9 - 1.0
Contribution value

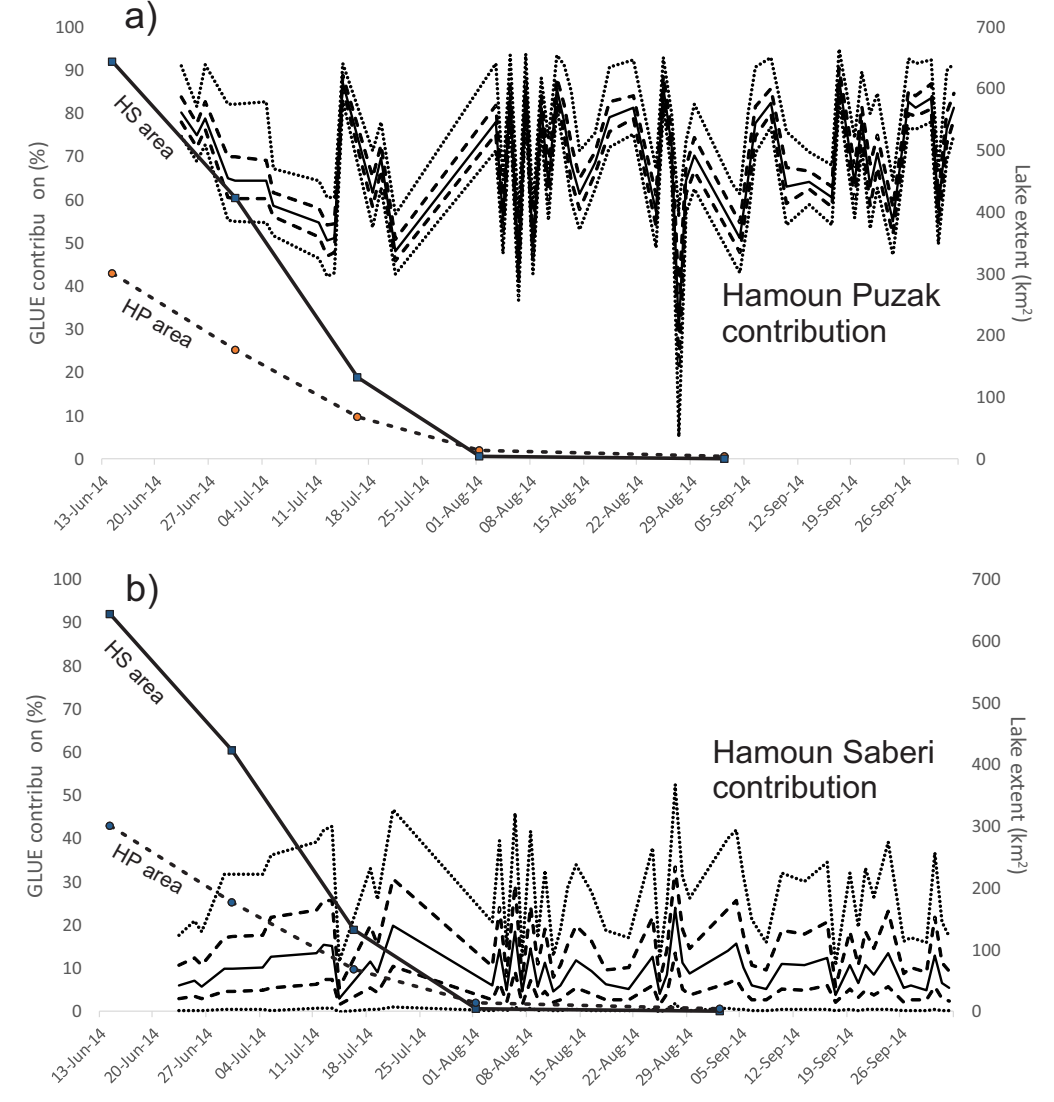
a)
HS area
HP area
Hamoun Puzak contribution
GLUE contribu on (%)
Lake extent (km²)
b)
HS area
HP area
Hamoun Saberi contribution
GLUE contribu on (%)
Lake extent (km²)
13-Jun-14
20-Jun-14
27-Jun-14
04-Jul-14
11-Jul-14
18-Jul-14
25-Jul-14
01-Aug-14
08-Aug-14
15-Aug-14
22-Aug-14
29-Aug-14
05-Sep-14
12-Sep-14
19-Sep-14
26-Sep-14

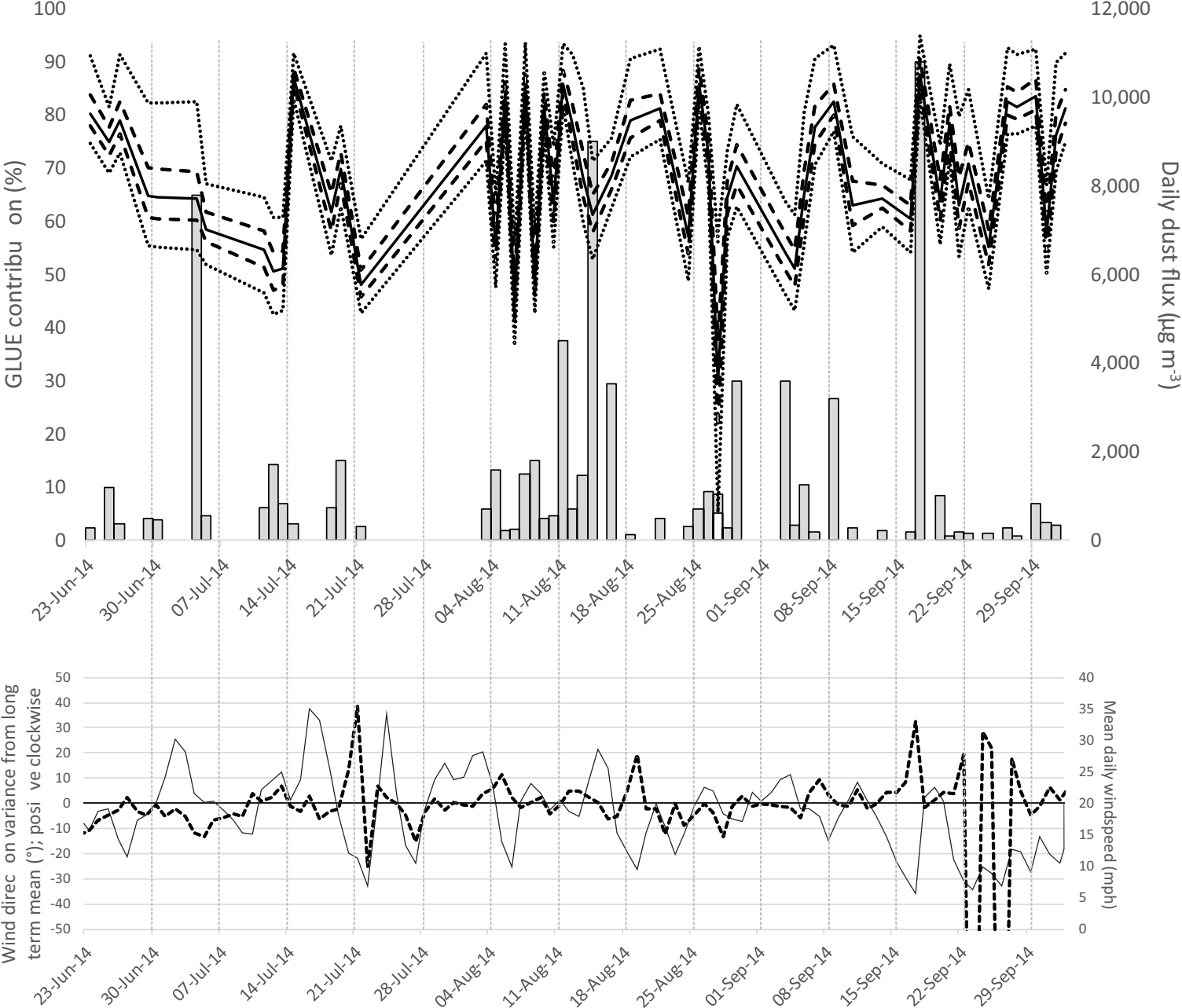
GLUE contribu on (%)
Daily dust flux (µg m-3)
100
90
80
70
60
50
40
30
20
10
0
12,000
10,000
8,000
6,000
4,000
2,000
0
23-Jun-14
30-Jun-14
07-Jul-14
14-Jul-14
21-Jul-14
28-Jul-14
04-Aug-14
11-Aug-14
18-Aug-14
25-Aug-14
01-Sep-14
08-Sep-14
15-Sep-14
22-Sep-14
29-Sep-14
Wind direc on variance from long term mean (°); posi ve clockwise
Mean daily windspeed (mph)
50
40
30
20
10
0
-10
-20
-30
-40
-50
40
35
30
25
20
15
10
5
0

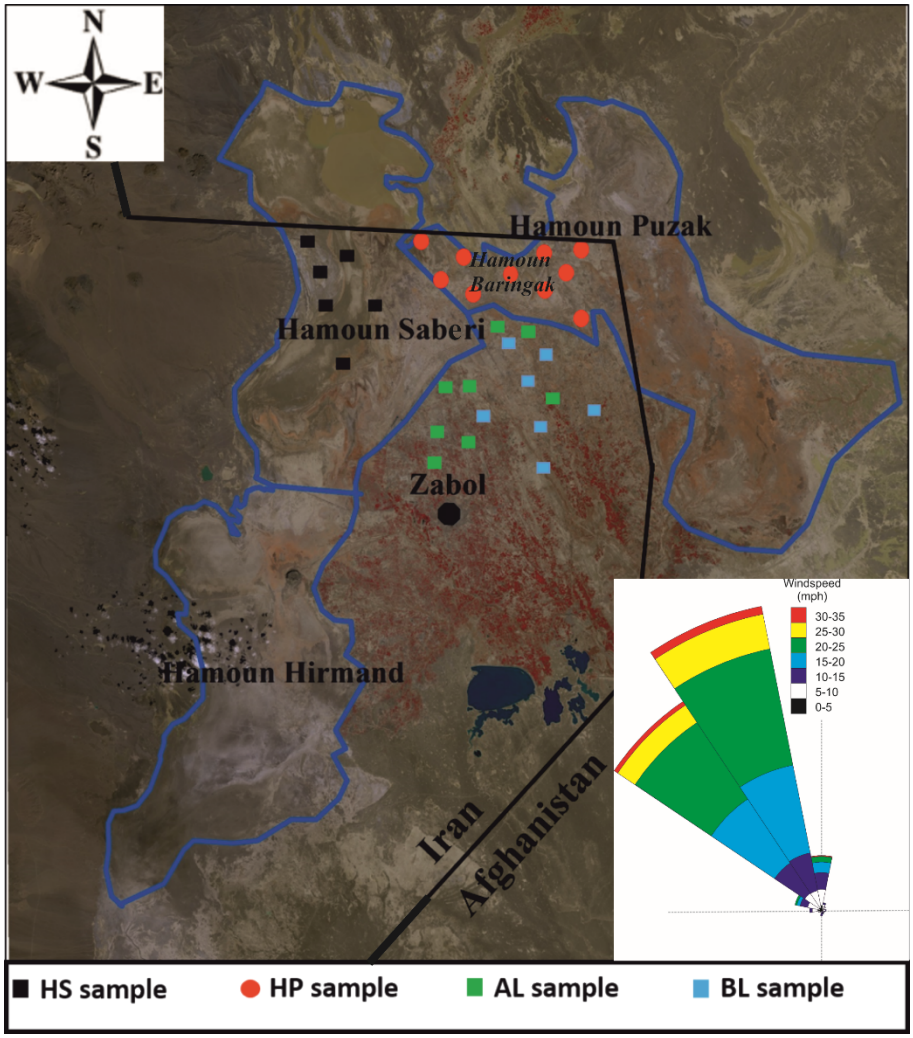
N
W
E
S
Hamoun Puzak
Hamoun Baringak
Hamoun Saberi
Zabol
Hamoun Hirmand
Iran
Afghanistan
Windspeed (mph)
30-35
25-30
20-25
15-20
10-15
5-10
0-5
HS sample
HP sample
AL sample
BL sample

Figure 1

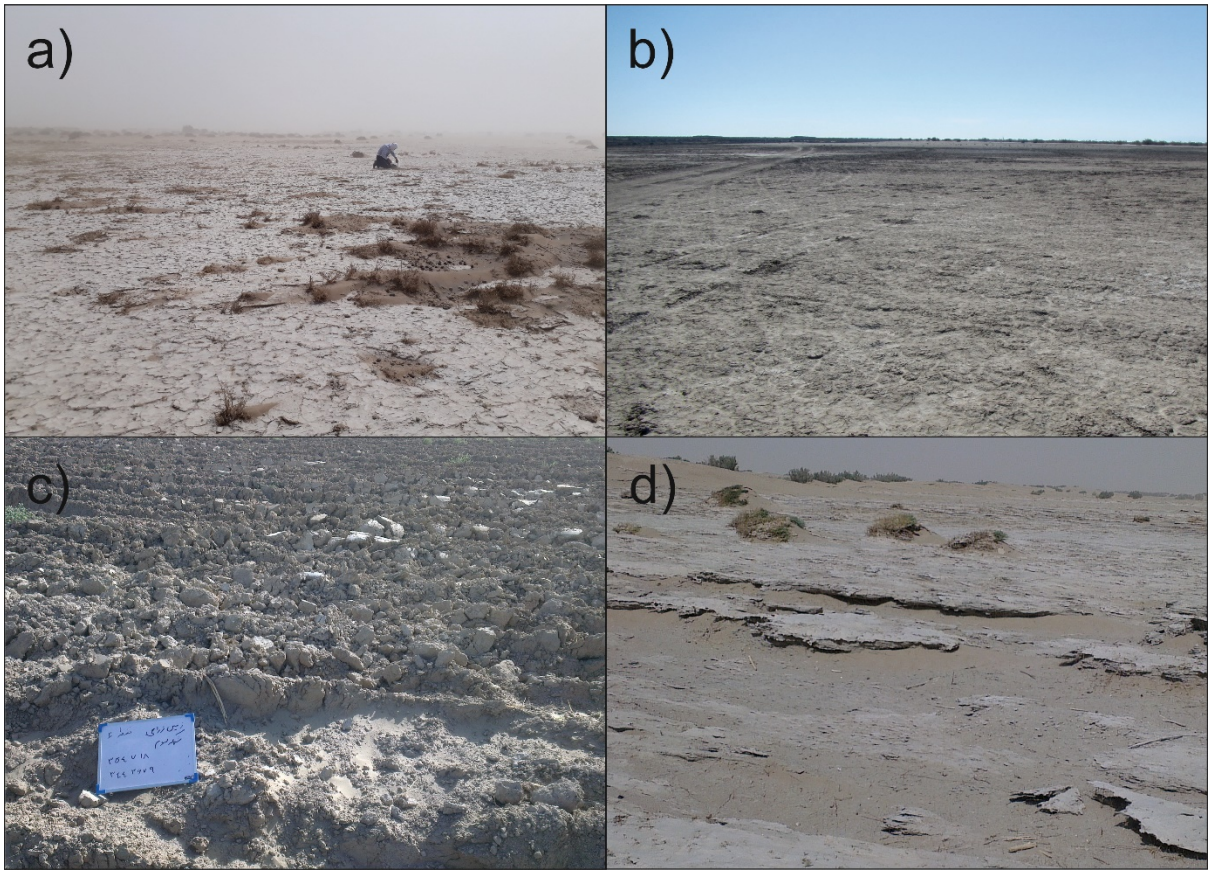

Figure 2.

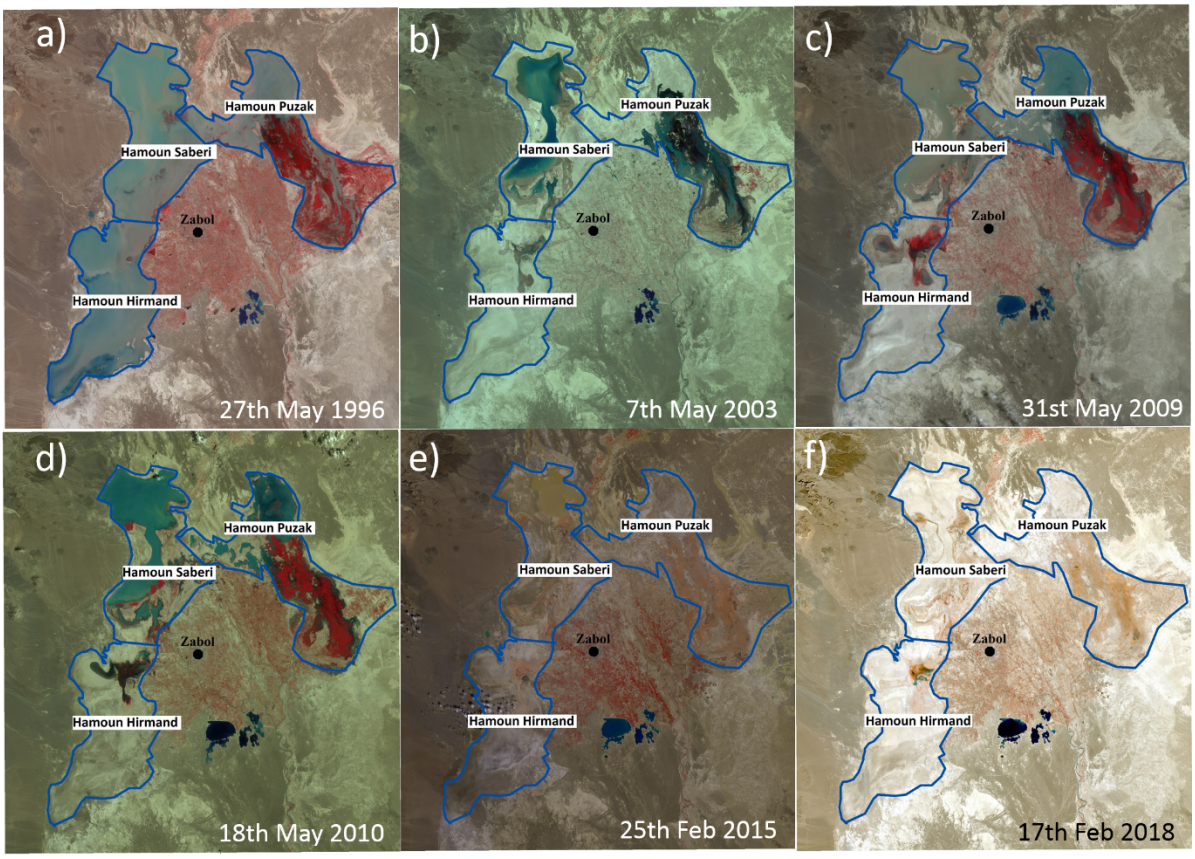
a)
Hamoun Puzak
Hamoun Saberi
Zabol
Hamoun Hirmand
27th May 1996
b)
Hamoun Puzak
Hamoun Saberi
Zabol
Hamoun Hirmand
7th May 2003
c)
Hamoun Puzak
Hamoun Saberi
Zabol
Hamoun Hirmand
31st May 2009
d)
Hamoun Puzak
Hamoun Saberi
Zabol
Hamoun Hirmand
18th May 2010
e)
Hamoun Puzak
Hamoun Saberi
Zabol
Hamoun Hirmand
25th Feb 2015
f)
Hamoun Puzak
Hamoun Saberi
Zabol
Hamoun Hirmand
17th Feb 2018

Figure 6.

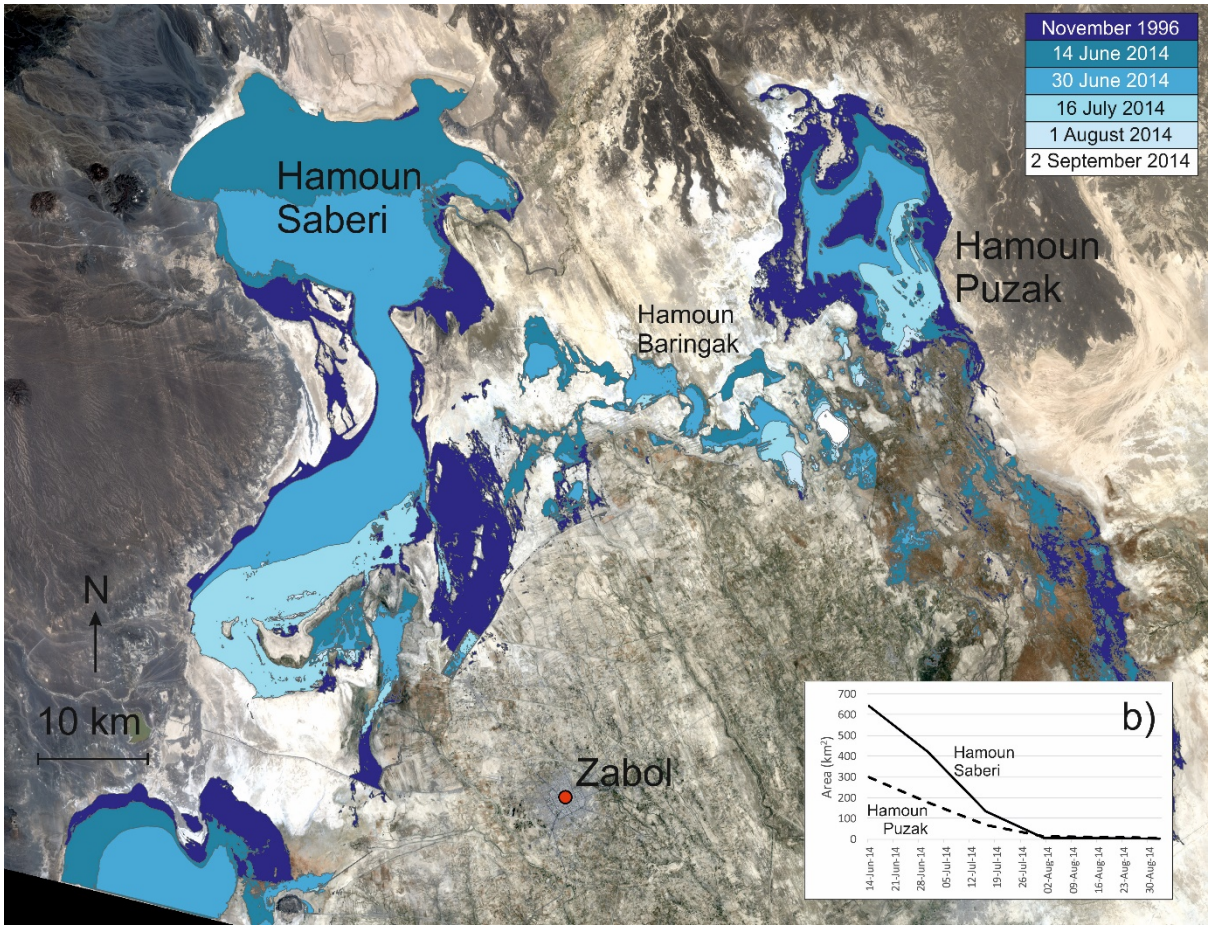
November 1996
14 June 2014
30 June 2014
16 July 2014
1 August 2014
2 September 2014
Hamoun
Saberi
Hamoun
Puzak
Hamoun
Baringak
N
10 km
Zabol
b)
Area (km²)
700
600
500
400
300
200
100
0
Hamoun
Saberi
Hamoun
Puzak
14-Jun-14
21-Jun-14
28-Jun-14
05-Jul-14
12-Jul-14
19-Jul-14
26-Jul-14
02-Aug-14
09-Aug-14
16-Aug-14
23-Aug-14
30-Aug-14

Figure 7.

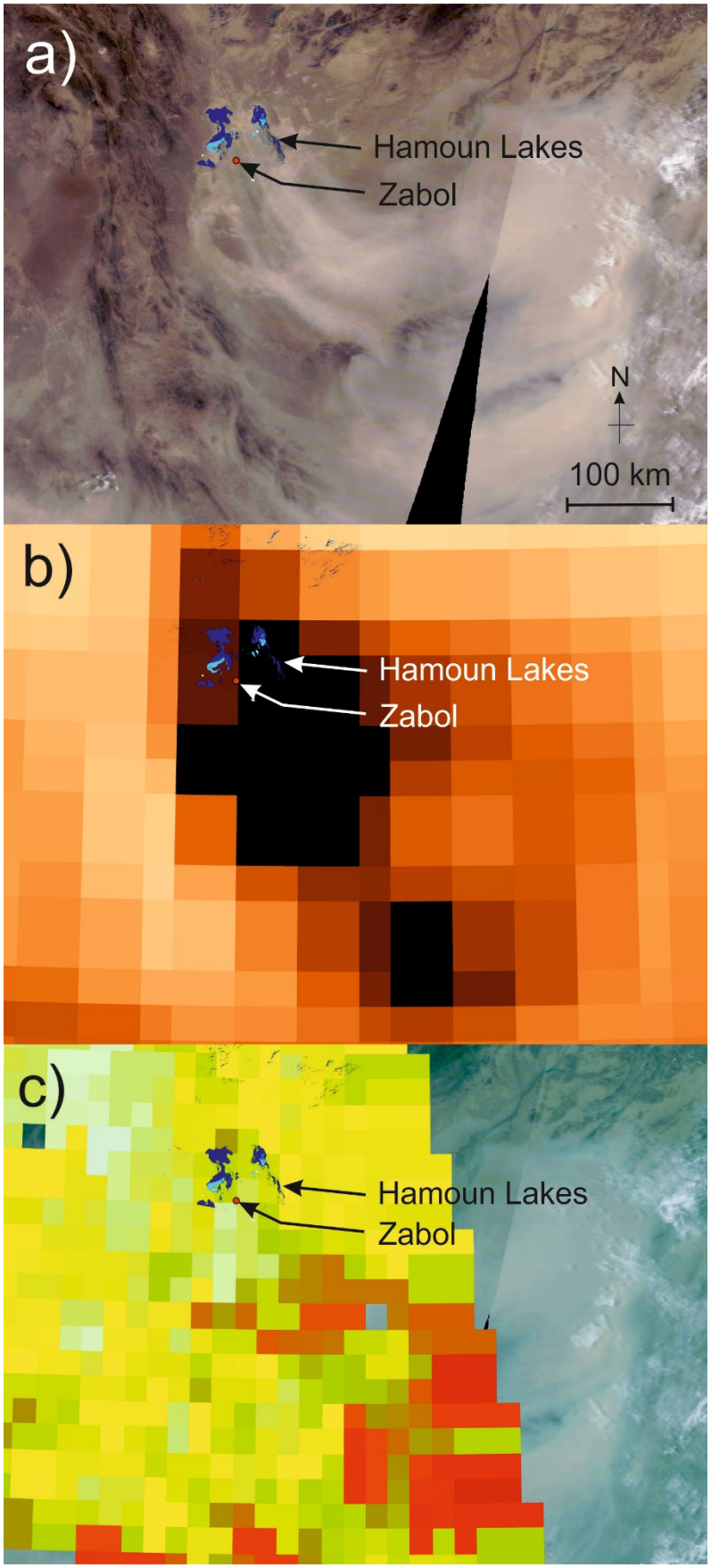
a)
Hamoun Lakes
Zabol
N
100 km
b)
Hamoun Lakes
Zabol
c)
Hamoun Lakes
Zabol

Figure 10.

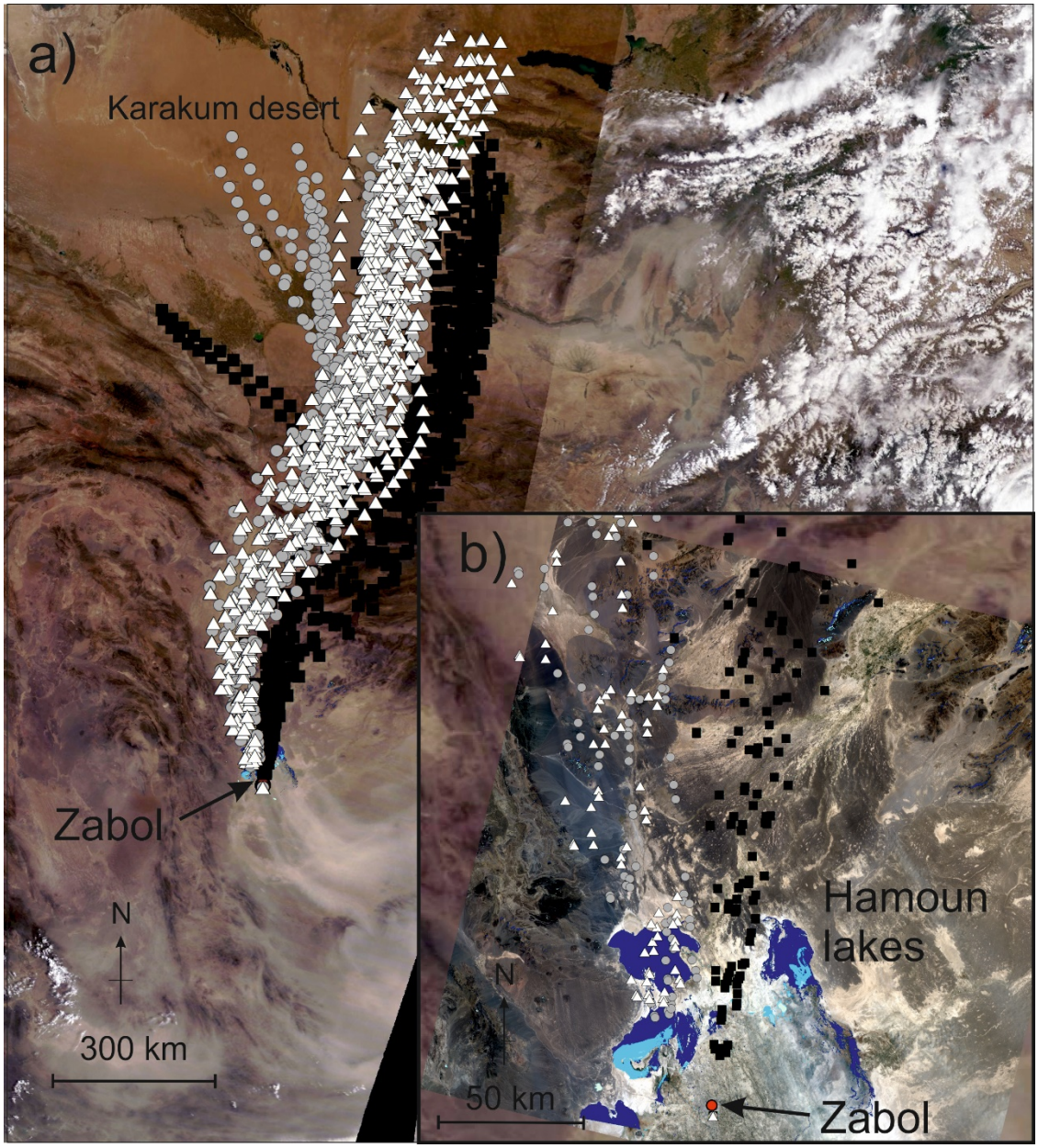

Figure 11.

CRediT Author statement

Reza Dahmardeh Behrooz: Software, Formal Analysis, Investigation, Visualization, Writing – Original Draft Preparation. **Hamid Gholami:** Software, Formal Analysis, Investigation, Visualization , Writing – Original Draft Preparation Supervision, Project Administration. **Matt W. Telfer:** Formal Analysis, Investigation, Visualization , Writing – Review & Editing. **John D. Jansen:** Investigation, Visualization, Writing – Review & Editing. **Abolhassan Fathabadi**: Conceptualization, Supervision, Project Administration